**Atmospheric
Chemistry
and Physics**

Glassy aerosols with a range of compositions nucleate ice heterogeneously at cirrus temperatures

T. W. Wilson[1,2], **B. J. Murray**[1], **R. Wagner**[3], **O. Möhler**[3], **H. Saathoff**[3], **M. Schnaiter**[3], **J. Skrotzki**[3], **H. C. Price**[1], **T. L. Malkin**[1], **S. Dobbie**[1], **and S. M. R. K. Al-Jumur**[1]

[1]School of Earth and Environment, University of Leeds, UK
[2]School of Chemistry, University of Leeds, UK
[3]Institute for Meteorology and Climate Research, Karlsruhe Institute of Technology, Germany

Correspondence to: B. J. Murray (b.j.murray@leeds.ac.uk)

Abstract. Atmospheric secondary organic aerosol (SOA) is likely to exist in a semi-solid or glassy state, particularly at low temperatures and humidities. Previously, it has been shown that glassy aqueous citric acid aerosol is able to nucleate ice heterogeneously under conditions relevant to cirrus in the tropical tropopause layer (TTL). In this study we test if glassy aerosol distributions with a range of chemical compositions heterogeneously nucleate ice under cirrus conditions. Three single component aqueous solution aerosols (raffinose, 4-hydroxy-3-methoxy-DL-mandelic acid (HMMA) and levoglucosan) and one multi component aqueous solution aerosol (raffinose mixed with five dicarboxylic acids and ammonium sulphate) were studied in both the liquid and glassy states at a large cloud simulation chamber. The investigated organic compounds have similar functionality to oxidised organic material found in atmospheric aerosol and have estimated temperature/humidity induced glass transition thresholds that fall within the range predicted for atmospheric SOA. A small fraction of aerosol particles of all compositions were found to nucleate ice heterogeneously in the deposition mode at temperatures relevant to the TTL (< 200 K). Raffinose and HMMA, which form glasses at higher temperatures, nucleated ice heterogeneously at temperatures as high as 214.6 and 218.5 K respectively. We present the calculated ice active surface site density, n_s, of the aerosols tested here and also of glassy citric acid aerosol as a function of relative humidity with respect to ice (RH$_i$). We also propose a parameterisation which can be used to estimate heterogeneous ice nucleation by glassy aerosol for use in cirrus cloud models up to ~ 220 K. Finally, we show

that heterogeneous nucleation by glassy aerosol may compete with ice nucleation on mineral dust particles in mid-latitudes cirrus.

1 Introduction

The effect of aerosol composition and state on cirrus cloud formation is poorly quantified. Cirrus clouds are ubiquitous throughout the upper troposphere and are known to have a significant impact on Earth's climate (Baker, 1997; Liou, 1986). The microphysical properties of cirrus in the extremely cold (180–200 K) tropical tropopause layer (TTL) have received significant attention in recent years (Peter et al., 2006). These cirrus are known to play a critical role in dehydrating air entering the stratosphere (Holton and Gettelman, 2001; Jensen et al., 1996) and may also have a non-negligible radiative impact on the planet (McFarquhar et al., 2000). The TTL is the region between 20° N and 20° S in which the tropopause is at its highest altitudes (14–18.5 km) (Fueglistaler et al., 2009). Cirrus which forms in situ in the TTL, rather than as the product of convective outflow, is horizontally extensive (up to 10^5 km^2), but very thin (200–300 m deep) (Lynch et al., 2002). These clouds have very low particle number densities (Krämer et al., 2009) making them optically thin and as such they are referred to as sub-visible or sub-visual cirrus (SVC) clouds. Observations in-situ indicate there is often significant supersaturation with respect to ice within these clouds (Peter et al., 2006; Krämer et al., 2009), but only very rarely higher than the homogeneous

ice nucleation threshold (Krämer et al., 2009). Such observations were unexpected as the presence and growth of ice particles was expected to quench any supersaturation (Peter et al., 2006).

A number of potential mechanisms for the sustained supersaturations observed in SVC have been suggested. Laboratory experiments have shown that a metastable phase of ice, originally described as cubic ice, can crystallise from aqueous droplets at TTL temperatures (Murray et al., 2005; Murray and Bertram, 2007, 2008; Murray, 2008a). More recent work has revealed that it is better described as stacking disordered ice (ice I_{sd}) (Malkin et al., 2012). This phase of ice has a higher vapour pressure than the stable hexagonal polymorph (Murray et al., 2005; Shilling et al., 2006a) and may allow a Bergeron-Findeisen like process, leading to a low ice number density. Gao et al. (2004) suggested that the adsorption of nitric acid onto ice particles can interfere with the uptake of water vapour, leading to supersaturations. It has also been proposed that inorganic acids may form coatings on frozen solution droplets that could slow the rate of ice particle growth (Bogdan and Molina, 2009, 2010). Magee et al. (2006) suggest that the uptake of water vapour by ice crystals in the TTL might be slow if the accommodation coefficient of water on ice is very small (< 0.0075). However, more recently the accommodation coefficient has been reported to be > 0.1 at temperatures between 190 and 225 K (Skrotzki, 2012). Barahona and Nenes (2011) have suggested that gravity wave activity in the TTL might lead to a "dynamic equilibrium" in which ice production balances sedimentation resulting in low ice number densities and high in-cloud humidity. In their study it was found that dynamic equilibrium was achievable when aerosol droplets froze homogeneously, but it was also found that heterogeneous nucleation by ice nuclei (IN) facilitated the onset of the equilibrium state.

A number of modelling studies show that the heterogeneous nucleation of ice in the absence of gravity waves can result in low particle densities and correspondingly long relaxation times for humidity (Krämer et al., 2009; Gensch et al., 2008; Khvorostyanov et al., 2006; Spichtinger and Gierens, 2009; Spichtinger and Cziczo, 2010; Jensen et al., 2010; Ren and Mackenzie, 2005; Murray et al., 2010b). Measurements of the composition of unfrozen background aerosol in the TTL and the composition of residues from evaporated SVC ice particles show very low concentrations of species traditionally considered to be effective IN, such as mineral dusts. Aerosol and ice particle residues are shown instead to be largely composed of neutralised sulphate-organic mixtures, the organic component being highly oxidised (Froyd et al., 2009a, 2010). DeMott et al. (2003) show that at warmer temperatures (218–238 K), mineral dust makes up a much larger fraction (33 %) of the IN which nucleated ice particles heterogeneously, despite them only making up a small percentage of the background aerosol (1 %, including fly ash). DeMott et al. (2003) also showed that 25 % of the heterogeneous ice residues were composed of

sulphate-organic residues, suggesting that organic-sulphate particles are significant heterogeneous ice nuclei.

Crystalline ammonium sulphate particles have been shown to nucleate ice heterogeneously and it has been suggested that they could influence cirrus formation (Abbatt et al., 2006; Wise et al., 2009, 2010; Eastwood et al., 2009; Jensen et al., 2010). However, a recent study has shown that citric acid, a glass forming organic tri-carboxylic acid, inhibits the efflorescence of ammonium sulphate below 250 K, making it unclear how many crystalline ammonium sulphate particles exist in the TTL (Bodsworth et al., 2010).

The effect of chemical composition on the physical state of atmospheric aerosols and the subsequent effect of aerosol state on ice nucleation are not currently well understood. In addition to the familiar liquid and crystalline states, atmospheric aerosol may also exist in semi-solid and solid amorphous states (i.e. lacking an ordered, repeating structure) such as rubbers, gels or glasses (Mikhailov et al., 2009). Aqueous solutions of surrogates for the highly oxidised organic species found in atmospheric aerosol have been shown to become glassy solids at humidities and temperatures relevant to a large part of the Earth's atmosphere (Murray, 2008b; Zobrist et al., 2008; Mikhailov et al., 2009). Glasses are amorphous solids with extremely high viscosities; liquids are considered to have become glasses if their viscosity exceeds 10^{12} Pa s (Angell, 1995; Debenedetti and Stillinger, 2001). Murray et al. (2012a) present visual evidence of glass or semi-solid formation in micrometer sized amorphous iodic acid droplets at low humidity. In their work, droplets were subjected to mechanical force and shattered in a manner consistent with a brittle glass. On humidification, the shattered droplets took up water, returned to the liquid phase and re-formed into droplets. Lower temperatures, higher solute concentrations and larger solute molecules capable of hydrogen bonding all serve to increase solution viscosity. The high mass oxygenated organic compounds found in atmospheric aerosol are therefore likely to increase viscosity and promote glass formation under atmospherically relevant conditions.

Evidence for natural aerosols existing in a solid amorphous state has been found in a number of studies. Cappa et al. (2011) found that heating ozone oxidised α-pinene aerosol did not lead to a change in the aerosol's mass spectra, which is not predicted by absorptive partitioning theory, indicating that the diffusion of molecules out of the aerosol was retarded. Similarly Vaden et al. (2011) found that the rate of evaporation of secondary organic aerosol (SOA) at room temperature was much slower than predicted by current kinetic models. Both Cappa and Wilson (2011) and Vaden et al. (2011) conclude that their observations are consistent with aerosol existing in an amorphous solid rather than a liquid state. Shiraiwa et al. (2011) found that the chemical aging of an organic aerosol proxy slows at lower humidity and they attribute this to the aerosol particles becoming semi-solid, which slows diffusion into the interior of the particles, reducing the reactive uptake. Virtanen et al. (2010) show

that a large proportion of SOA generated in a plant chamber and aerosol sampled from boreal forest bounced off an impactor, behaviour which is consistent with amorphous solid rather than liquid aerosol. They state that the tested SOA was most probably glassy. Measurements using a similar technique show that laboratory generated SOA remained solid or semi-solid at up to at least 50 % relative humidity with respect to liquid water. The same study found that the addition of sulphuric acid to the SOA resulted in a reduction in the humidity at which the aerosols liquefied due to their increased hygroscopicity (Saukko et al., 2012).

As discussed by Koop et al. (2011), other atmospheric measurements have also shown that some carbonaceous aerosols emitted during biomass burning exist in amorphous solid or semi-solid states. These spherical particles behave like solids and are referred to as "tar balls" (Posfai et al., 2004; Tivanski et al., 2007; Alexander et al., 2008). The number of tar balls increases as biomass burning plumes age (Adachi and Buseck, 2011), which is likely to be related to ongoing oligomerisation reactions between poly-carboxylic acids that result in heavier molecules, which promote higher viscosities. Tar balls have been found to have much in common with humic-like complex organic acids, which have been shown to have very high glass transition temperatures (Young and Leboeuf, 2000). Anthropogenic aerosol may also exist as an amorphous solid; Roth et al. (2005) suggest that up to 80 % of urban organic particulates may be in the glassy state, based on the sorption behaviour of volatile organic compounds. They suggest that this is likely due to the presence of oligomeric species in the aerosol.

Murray (2008b) and Zobrist et al. (2008) simultaneously proposed that the homogeneous freezing of high viscosity or glassy oxidised organic solution aerosol may be delayed or inhibited. However, cloud chamber experiments showed that rather than inhibiting ice formation, glassy citric acid aerosols behaved as heterogeneous ice nuclei at temperatures lower than 208 K (Murray et al., 2010b). The aim of the experiments presented in this paper was to test whether the ability to nucleate ice heterogeneously is a common property of glassy aerosols, independent of chemical composition. In this study we tested to see if aerosols of four different chemical compositions nucleated ice in the deposition mode. All of the aerosols that were examined become glassy under upper tropospheric conditions. A useful measure of an aqueous solution's ability to form a glass is the temperature at which the glass transition occurs when the surrounding environment is at ice saturation. This is given the symbol T_g' (Zobrist et al., 2008). It is a useful quantity as it provides a means of comparing different solutes glass forming abilities under common atmospherically relevant conditions. Two of the aqueous systems that were studied, levoglucosan and a multi-component aerosol (raffinose/M5AS, M5AS = five dicarboxylic acids plus ammonium sulphate), have T_g' values close to that of citric acid. The other two systems, raffinose and 4-hydroxy-3-methoxy mandelic acid (HMMA),
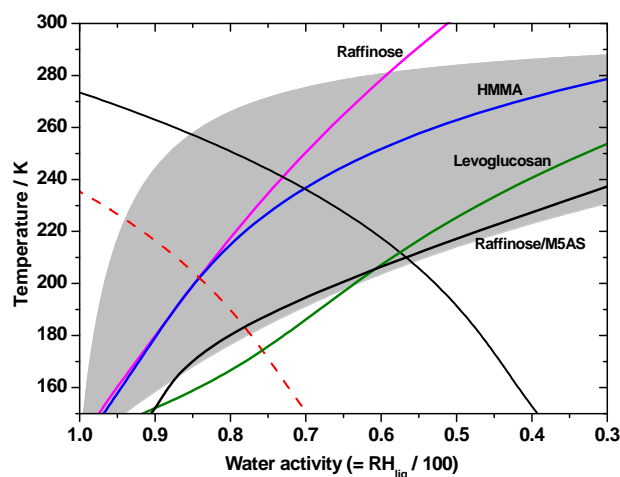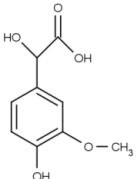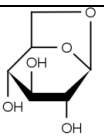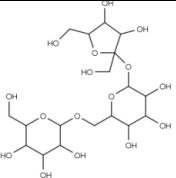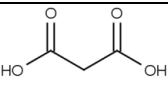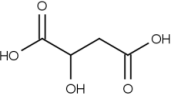

Fig. 1. An aerosol state diagram comparing the estimated range of the relative humidity induced glass transition threshold (RH_g) for atmospheric SOA (grey area) (Koop et al., 2011) and the RH_g thresholds (Zobrist et al., 2008) for the aerosols investigated in this study. The solid black line is the ice-liquid equilibrium and the dashed red line is the homogeneous freezing threshold for liquid solution droplets (Koop et al., 2000). All the aerosols t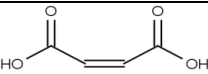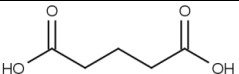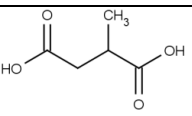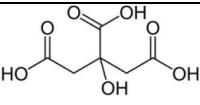ested have T_g' values (the point at which RH_g and the ice liquid equilibrium intersect) in the range predicted for SOA, indicating that they are reasonable surrogates for glassy atmospheric SOA. For a more detailed explanation of aerosol state diagrams see Sect. 2.1.

have much higher T_g' values (see Table 1 for a comparison of their molecular structures and T_g').

These substances were chosen for study partly because their chemical functionality is diverse and they are well characterised systems, but also because they are broadly representative of organic atmospheric aerosol. The T_g' values of the aerosols chosen for study all fall within the range predicted for atmospheric SOA (Fig. 1) (Koop et al., 2011) based upon the chemical properties of SOA derived from measurements made during the AMAZE-08 campaign (Gunthe et al., 2009). Levoglucosan ($C_6H_{10}O_5$), a monosaccharide anhydride, is a major component of biomass burning aerosol and has been observed to make up as much as 60 % of the mass of aerosol from particular types of combusted biomass (Iinuma et al., 2007; Knopf and Rigg, 2011). Raffinose ($C_{18}H_{32}O_{16}$), a trisaccharide, has also been identified as a component of biomass burning aerosol (Decesari et al., 2006; Wan and Yu, 2007). HMMA ($C_9H_{10}O_5$) is an aromatic compound that is used as a surrogate for the water soluble organic compounds found in atmospheric aerosol (Decesari et al., 2006). Raffinose/M5AS is a multi-component oxidised organic/sulphate mixture and more closely represents internally mixed atmospheric aerosol found in the TTL. The water activity and glass transition curves of all four atmospheric proxies used here are taken from Zobrist et al. (2008).

Table 1. Molecular structures of the glass forming components of the four aqueous aerosols examined in this study with associated T_g' and uncertainties (Zobrist et al., 2008). The molecular structure and T_g' of citric acid, a component of glassy aerosol previously tested by Murray et al. (2010b) has been included for comparison (note that no uncertainties in T_g' were available for citric acid). The bracketed percentages next to the components of raffinose/M5AS aerosol indicate the individual species contribution by mass to the mixture.

Aerosol	Component(s)	Molecular structure	T_g' / K	± / K
HMMA	4-Hydroxy-3-methoxy-DL-mandelic acid		236.5	3.5
Levoglucosan	(-)-1,6-Anhydro-β-D-glucopyranose		211.7	11.1
Raffinose	D-(+)-Raffinose pentahydrate		240.6	6.1
Raffinose/M5AS	D-(+)-Raffinose pentahydrate (50.00 %)	See above	209.6	8.1
	Malonic acid (15.35 %)			
	DL-Malic acid (7.35 %)			
	Maleic acid (7.05 %)			
	Glutaric acid (8.85 %)			
	Methylsuccinic acid (3.70 %)			
	Ammonium sulphate (7.70 %)	$(NH_4)_2SO_4$		
Citric acid	Citric acid		211.8	-

2 Methodology

In order to quantify ice nucleation by glassy aerosol, experiments were performed at the AIDA (Aerosol Interactions and Dynamics in the Atmosphere) chamber at the Karlsruhe Institute of Technology, Germany. The AIDA chamber is a large (84 m^3), highly instrumented aerosol and cloud chamber in which the temperatures and humidities necessary for cirrus formation are accessible. The operation of the AIDA chamber during deposition mode ice nucleation experiments has been described in detail in the past (Möhler et al., 2006; Wagner et al., 2010) and will only be briefly discussed here.

The temperature of the aluminium walls of the chamber was controlled between $\sim$ 190 and 240 K during this study. This was achieved by using liquid nitrogen to cool air within the chamber's thermostated jacket. The gas phase water partial pressure (P_{H_2O}) in the chamber was controlled by a coating of ice on the vessel walls. The ice layer was deposited after the chamber had been evacuated to $\sim$ 0.01 hPa and then flushed repeatedly with particulate free air to reduce the number of background aerosol particles to < 1 cm^{-3}. Purified water was evaporated into the evacuated chamber, which deposited as an ice layer on the cooled chamber walls. Temperature sensors arranged vertically and horizontally in the chamber determined the average gas temperature and are embedded in the aluminium walls to determine the average wall temperature. The chamber was continuously stirred by a fan and the measured gas temperatures are typically within ±0.3 K (Wagner et al., 2011). The presence of internal sources of heat (heated sampling tubes, the mixing fan etc.) meant that the gas temperature was slightly higher than the wall temperature, giving a relative humidity with respect to hexagonal ice (RH$_i$ = $p_{H_2O}/p_{ice}(T) \times 100$, where $p_{ice}(T)$ is the equilibrium vapour pressure over a flat surface of hexagonal ice) of around 90–95 % at equilibrium. The equilibrium vapour pressure over a flat surface of hexagonal ice was calculated from the mean gas temperature using the parameterisation from Murphy and Koop (2005).

In order to produce supersaturated conditions, the pressure in the chamber was reduced by pumping air out of the chamber using a pair of vacuum pumps. Heat conduction from the walls into the chamber was relatively slow and the expansion was initially close to adiabatic. This results in a decrease in the gas temperature, which causes the RH$_i$ to increase. The gas phase water partial pressure (p_{H_2O}) was determined using absorption measurements from a multipath cell tuneable diode laser (TDL) spectrometer (Wagner et al., 2010). Measurements of p_{H_2O} using this system are found to be within 5 % of the actual value (Skrotzki, 2012; Fahey et al., 2009). The total water content (ice and gas phases) was determined using a chilled mirror hygrometer (MBW LX-373) which sampled gas from the chamber via a heated tube, returning any sampled ice particles to the gas phase (Wagner et al., 2009, 2010, 2011).

An aqueous aerosol dispersion of the desired composition was introduced into the chamber by nebulising 3–3.5 wt % bulk solutions with a compressed-air atomiser. The aerosol particle concentration reached an almost constant value of about 1.5×10^4 cm^{-3} shortly after nebulising. Aerosol number concentrations were measured using condensation particle counters (CPC, TSI 3010, 3775, 3776). The CPC3010 was used at pressures below ambient, allowing the aerosol number concentration to be measured continuously during expansion experiments. However, CPC3010 was unavailable for some experiments; in these cases two other CPC instruments (CPC3775 and CPC3776) were used. These instruments are only able to operate at ambient pressure so just prior to each expansion the aerosol number concentration was measured for a period of time ($\sim$ 200 s). The aerosol concentration falls continuously even when not expanding because of sampling losses and deposition of particles to the walls. To account for this, a linear fit to the mean of the CPC3775 and CPC3776 concentration/time data was extrapolated to the time at which the expansion started. This estimated initial aerosol concentration was then scaled with the decreasing chamber pressure during expansion, providing an estimate of the aerosol number concentration during the experiments. This estimate was compared with data from experiments that used CPC3010 and was found to be accurate to within 3–10 %. The aerosol concentration during expansion experiments was typically 5000–15 000 cm^{-3}.

The aerosol size distributions were measured using both an aerodynamic particle sizer (APS, TSI) and a scanning mobility particle sizer (SMPS, TSI) (Fig. 2). A particle density of 1.6 g cm^{-3} was assumed when converting the aerodynamic diameters measured by the APS into volume-equivalent spherical diameters (d_p) (Hinds, 1999). The exact densities of the solution aerosol used are unknown, however the assumed density is close to that of the crystalline forms of the species investigated. Spherical particles have mobility-equivalent diameters (as measured by the SMPS) that are equal to d_p. The aerosols used in this campaign had a mean d_p of around 0.170 μm.

The onset of ice nucleation was observed in-situ using the laser scattering and depolarisation instrument SIMONE (Schnaiter et al., 2012). Three photomultipliers mounted outside the chamber's thermal housing receive forward and back scattered light (I_{for}; 2° to the incident beam, I_{back}; 178° to the incident beam). The incident continuous wave laser beam has an emission wavelength of 488 nm and is linearly polarised with its polarisation vector oriented parallel to the scattering plane. Light scattered in the 178° direction is decomposed according to its polarisation state by means of a polarising prism. The intensities of the scattered components having a polarisation parallel to ($I_{back,par}$) and perpendicular to ($I_{back,per}$) the scattering plane are measured. The backscattering linear depolarisation ratio, δ, is then defined as the ratio of $I_{back,per}$ to $I_{back,par}$. The magnitude of δ is dependent on particle size and shape; for perfectly spherical particles, δ
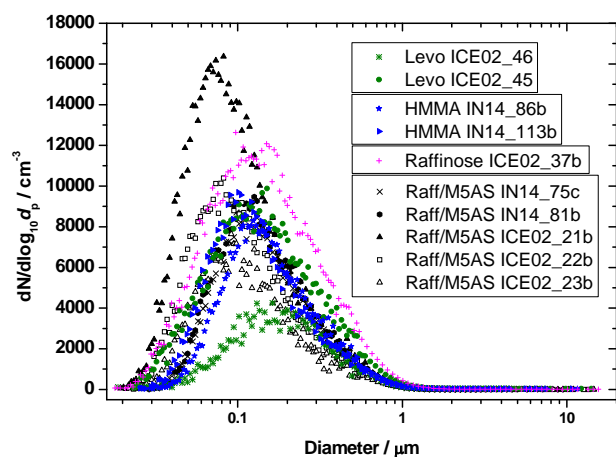
Fig. 2. A comparison of size distributions of aerosols taken immediately prior to experiments shown in Fig. 7. The average of the mean volume-equivalent sphere diameters (d_p) of the aerosols was $0.170 \pm 0.027\,\mu m$.

would be zero, in practice the observed δ for unfrozen glassy aerosols and liquid aerosols in this study was between 0.02 and 0.03. This small background δ was due to a combination of the incident laser light being only 99 % linearly polarised to start with, Rayleigh scattering by air molecules and minor optical misalignments. Ice particles are aspherical and cause a clear increase in δ. A change of at least 1 % was used to infer the onset of ice nucleation (see Sect. 3.1 for an example of the change in δ during an ice nucleation experiment) (Möhler et al., 2003; Schnaiter et al., 2012).

Two WELAS2000 optical particle counters (Palas GmbH) were used to count and size single particles. These instruments have already been described in detail elsewhere (Benz et al., 2005; Wagner et al., 2006). Each instrument measures a different size range for spherical particles with the refractive index of ice (1.33); WELAS 1 covers 0.7–46.0 µm and WELAS 2 covers 5.0–240.0 µm. The optical sizes for aspherical particles (e.g. ice crystals) should be considered approximate as particle asphericity is not considered when relating the scattering intensity to particle diameter. The total particle number concentration measured with the WELAS 1 instrument is used to infer ice particle number concentrations (N_{ice}) by applying a threshold size above which particles are assumed to be ice. In order to differentiate between ice particles and background aerosol the threshold has to be tuned depending on the size of the background aerosol and the rate of growth of the ice particles. At lower temperatures ice particles do not grow as large because of the lower absolute humidity. Consequently for experiments which took place below $\sim 200\,K$ it was not possible to apply a size threshold to distinguish ice crystals from the larger of the background aerosol particles.

In a companion paper we discuss the pre-activation of aqueous aerosol under conditions relevant for the present study (Wagner et al., 2012). Under specific conditions it was observed that aerosol particles which had already nucleated ice homogeneously would act as ice nuclei at around 105 % RH_i in subsequent expansions, even after being held under subsaturated conditions for in excess of 30 min between expansion experiments. Pre-activation was only observed in aerosol close to their predicted T'_g, so it was possible to design experiments in such a way as to avoid the aerosol becoming pre-activated. The results presented below for heterogeneous ice nucleation in the glassy regime are only for aerosols which had not been frozen homogenously prior to cooling or for aerosol which had been frozen homogeneously at temperatures too high for pre-activation to occur (which was confirmed by performing a second expansion at the same temperature to look for early ice nucleation). While this reduced the number of experiments that it was possible to perform within the time constraints of the campaign, it was necessary in order to unambiguously avoid experimental artefacts relating to pre-activation.

2.1 Aerosol state: glassy, liquid or crystalline

The four aqueous systems we selected for study have been characterised and the conditions under which they form glasses have been quantified (Zobrist et al., 2008). The state diagram for aqueous levoglucosan is shown in Fig. 3. Plotted in this diagram are the ice-liquid equilibrium threshold (solid black line) and the homogeneous freezing threshold (dashed red line), which are both related directly to water activity (Koop et al., 2000). The advantage of plotting the state diagram in terms of water activity as opposed to concentration is that at equilibrium, the water activity of liquid solution aerosol is equal to RH_{liq} (relative humidity with respect to liquid water). Hence, if an aerosol particle is able to come into equilibrium with its surroundings rapidly, then it is possible to estimate the aerosol's solute concentration based on temperature and RH_{liq}. However, if the aerosol particle is glassy or semi-solid, then diffusion of water into the particle will be slower and it may remain out of equilibrium, making the water activity no longer equal to the RH_{liq} (Mikhailov et al., 2009; Zobrist et al., 2011; Tong et al., 2011; Koop et al., 2011).

The glass transition for aqueous levoglucosan solution aerosol (solid green line) as a function of temperature and water activity is also plotted in Fig. 3. This is taken from fits to experimental data provided by Zobrist et al. (2008), which allowed the authors to calculate the solute specific constant, k, from the Gordon-Taylor equation (Eq. 1) for the glass transition temperature of binary solutions (Gordon and Taylor, 1952; Katkov and Levine, 2004). Using the value of k determined by Zobrist et al. (2008) ($k = 5.2$ for levoglucosan) and the glass transition temperatures of the pure form of each of the components of the solution (T_{g1} and T_{g2}), which in this
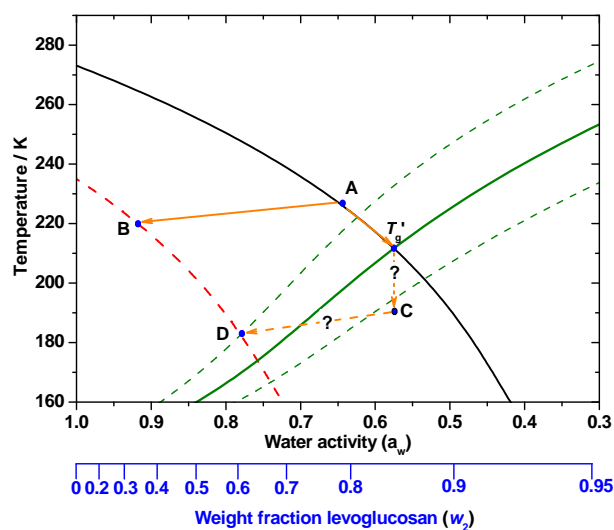
Fig. 3. The phase diagram of levoglucosan solution aerosol. The black line is the ice liquid equilibrium line, the dashed red line is the homogeneous freezing threshold based on the water activity homogeneous freezing criteria (Koop et al., 2000) and the green solid line is the humidity induced glass transition threshold (RH_g) for levoglucosan solution aerosol, with associated upper and lower uncertainties (dashed green lines) based on uncertainties in the parameters used in the Gordon-Taylor equation (Eq. 1) (Zobrist et al., 2008). The orange arrows represent idealised temperature/humidity trajectories. The ice-liquid equilibrium and homogeneous freezing lines are common to all solutions used in this study, but RH_g is unique to each solution system.

case are water ($T_{g1} = 136$ K, Johari et al., 1987; Kohl et al., 2005) and levoglucosan ($T_{g2} = 283.6$ K, Zobrist et al., 2008), the glass transition temperature T_g was calculated as a function of the weight fraction of levoglucosan (w_2). The weight fraction of water, w_1, is equal to $1 - w_2$. We have also plotted the upper and lower limits of T_g (dashed green lines) calculated using the estimated uncertainties in k and T_{g2}.

$$T_g(w_2) = \frac{w_1 T_{g1} + \frac{1}{k} w_2 T_{g2}}{w_1 + \frac{1}{k} w_2} \qquad (1)$$

The solute weight fraction could then be converted to water activity using a parameterisation provided by Zobrist et al. (2008), based on vapour pressure measurements taken for solutions of differing concentration at a series of temperatures between 313 and 289 K, which were then extrapolated to lower temperatures. As water activity is directly equivalent to relative humidity when at equilibrium, the calculated T_g thresholds can be used to estimate the humidity and temperature at which a liquid aerosol particle would become glassy and vice versa. We refer to the T_g threshold calculated here as the humidity induced glass transition, RH_g, as this is of relevance in our experiments as the aerosol are subject to a more significant change in humidity than temperature during expansions.

Under non-expansion conditions, the chamber water vapour is almost in equilibrium with the ice layer on the walls. Consequently, the water activity of aqueous liquid solution aerosols in the chamber, which are in equilibrium with the gas phase, is therefore approximately described by the ice-liquid equilibrium line shown in Fig. 3. The actual chamber humidity was around 90–95 % RH_i, due to the presence of heat sources in the chamber (as discussed above), so the exact water activity of liquid aerosol is to the right (lower water activity) side of the ice-liquid equilibrium line. For simplicity, we depict the trajectory of the change in temperature and water activity of aerosol particles during chamber cooling/heating periods as being along the ice-liquid equilibrium line. The point at which RH_g and the ice-liquid equilibrium line cross (T'_g) is a useful indication of the likely state of aerosol particles before an expansion experiment. Above T'_g, the aerosol particles are likely to be liquid and below they are likely to be in the glassy state.

Aerosol particles were injected into the chamber when the gas temperature was above T'_g of the aerosol type being investigated. These liquid solution droplets equilibrated with the water vapour in the chamber. The concentration of liquid levoglucosan solution aerosol injected at ~ 237 K rapidly adjusted to around point A in Fig. 3. Slow cooling (~ 4 K h^{-1}) of the chamber walls allowed the water vapour within the chamber to remain equilibrated with the ice film on the walls. The viscosity of liquid near the glass transition increases rapidly with decreasing temperature and decreasing water activity (Angell, 2002; Murray, 2008a, b). At around T'_g, the aerosol water content will cease to respond to changes in humidity. This is represented tentatively by the vertical dashed arrow in Fig. 3 between T'_g and point C.

The evolution of aerosol composition differs when an expansion is started in the liquid regime compared to the glassy regime. Liquid solution aerosol at point A (Fig. 3) take up water and dilute as the chamber humidity rises with decreasing temperature (arrow between points A and B). This increases the aerosol particles' water activity until ice nucleates at the homogeneous ice nucleation threshold (point B). The change in water activity on increasing humidity of a glassy aerosol starting at point C is not clear since the uptake of water is dependent on the rate at which water molecules can diffuse into the aerosol particles. The rate of diffusion of water in glassy solids is very slow (Koop et al., 2011; Tong et al., 2011; Zobrist et al., 2011) and once RH_g is crossed liquefaction of the aerosol particles may be delayed (Mikhailov et al., 2009; Tong et al., 2011). If the aerosol particles do liquefy then they will freeze at the homogeneous nucleation threshold at point D. Nevertheless, prior to liquefying these aerosol particles will exist in a glassy state while in an ice supersaturated environment.

There is some uncertainty in the conditions under which the aerosol particles exist in a glassy state and cease to be in equilibrium on slowly cooling the chamber. This is due

to uncertainty in the position of the RH_g line. In addition to the upper and lower uncertainty limits for RH_g, shown in Fig. 3 there is also an additional error in RH_g associated with the conversion of solution concentration to water activity, as it was necessary for Zobrist et al. (2008) to extrapolate measurements of solution water activity to low temperatures. Also, the enhancement of vapour pressure due to surface curvature (the Kelvin effect) can become important for small droplets. However, at 243.15 K a 100 nm pure water droplet would have a vapour pressure only 2.9 % higher than that of a flat surface of liquid water, suggesting that the Kelvin effect is of secondary importance. This was calculated using water density of 983.8 kg m^{-3} (Wagner and Pruss, 2002), a surface tension estimated using a parameterisation by Vargaftik et al. (1983) (which is consistent with nucleation data well below the temperatures at which surface tensions have been measured, Murray and Jensen, 2010) and a saturation vapour pressure for a flat water surface calculated using the parameterisation provided by Murphy and Koop (2005). Finally, it should also be noted that the conditions under which an aerosol particle will undergo the glass transition and go out of equilibrium with the surrounding atmosphere are time dependent. When given a longer equilibration time, a droplet will remain in equilibrium to lower temperatures and therefore greater concentrations. However, the viscosity of many aqueous solutions increases so strongly with decreasing temperature (because they are fragile liquids, which have much "sharper" glass transitions on cooling, Angell, 2002) that the glass transition temperature provides a very useful estimate of the conditions under which the dynamic arrest of the solution is expected.

At low temperatures, the solution droplets in the AIDA chamber are highly supersaturated with respect to their solutes' crystalline phases. For example, the solubility of raffinose at 273 K is 30 g l^{-1} (Hungerford and Nees, 1934) (and will decrease at lower temperatures), whereas the predicted aerosol composition when at ice saturation at 238 K (based on water activity data from Zobrist et al. (2008) is 782.5 g l^{-1}. Under similarly supersaturated conditions, oxalic acid or ammonium sulphate solution aerosol would be expected to slowly crystallise (Wagner et al., 2010, 2011; Abbatt et al., 2006). This is important because crystalline solid salts are known to catalyse ice nucleation (Wise et al., 2009, 2010; Abbatt et al., 2006; Baustian et al., 2010; Shilling et al., 2006b; Eastwood et al., 2009), as are crystalline hydrates (Wise et al., 2012). However, nucleation and crystal growth in highly viscous or glassy aqueous aerosol particles is much slower. For example, none of the species investigated in this study were observed to crystallise during the experiments carried out on droplet in oil emulsions by Zobrist et al. (2008). In single particle trap experiments at 298 K, 10 μm diameter levoglucosan particles did not crystallise when they were dried to < 5 % RH_{liq} over the course of minutes (Chan et al., 2005). Similarly, Mikhailov et al. (2009) showed that at 298 K, aqueous levoglucosan droplets of ∼ 100 nm diameters

did not crystallise in a differential mobility instrument at low RH_{liq} (5 %). X-ray diffraction measurements by Chatterjee et al. (2005) show no crystallisation of raffinose from freeze concentrated bulk solutions cooled initially to 203 K at 1 K per minute and then annealed at 241 K (T_g' for raffinose solution) for 8 h. This indicates that close to T_g', raffinose does not crystallise. At room temperature, Tong et al. (2011) found that amorphous raffinose particles held at ∼ 0 % RH_{liq} for approximately 6.5 h did not crystallise. In our companion study on the pre-activation behaviour of glassy aerosols (Wagner et al., 2012) freezing experiments conducted using 15 wt % raffinose solution in oil emulsions within a powder X-ray diffractometer showed that homogeneous ice nucleation in the droplets did not catalyse the crystallisation of the raffinose solute at 236 K.

The raffinose/M5AS aerosol used in this study was composed of raffinose, five dicarboxylic acids and ammonium sulphate. Nucleation of one crystalline phase from complex mixtures is likely to be further reduced as the presence of other solutes reduces the saturation with respect to any single compound. For example, Bodsworth et al. (2010) show that the addition of more than 30 % citric acid (by mass) to ammonium sulphate solution droplets inhibits their crystallisation at < 250 K. Even at room temperature, where crystallisation is expected to be more likely, droplets doped with more than 50 % citric acid did not crystallise.

The available literature data strongly suggests that the highly viscous solutions used in this study did not crystallise even though they were highly supersaturated. This is supported by the SIMONE depolarisation measurements made during the campaign. This technique was used in previous studies at AIDA to track crystallisation in oxalic acid aerosols with similar size distributions to those in this study (Wagner et al., 2010). Concomitant Fourier transform infrared spectroscopy (FTIR) measurements during experiments with the oxalic acid aerosol confirmed that the entire aerosol population had crystallised.

Liu and Mishchenko (2001) performed T-matrix calculations for polydisperse, randomly oriented spheroidal and cylindrical particles with a refractive index of 1.5. This refractive index is consistent with that of crystalline sucrose (1.558) (Tong et al., 2011) and is likely to be similar to that of the species used in this study. They present δ as a function of the effective equal-volume-sphere radius (r_{eff}) (Hansen and Travis, 1974) and the ratio of the spheroids/cylinders largest and smallest semi-axes. The change in δ that would be expected to result from the crystallisation of the aerosols used in this study, based on the calculations by Liu and Mishchenko (2001) was assessed. The particle size distributions shown in Fig. 2 were converted to r_{eff} values, which were then adjusted to account for the longer wavelength assumed by Liu and Mishchenko (2001) (603 nm) compared to that used by the SIMONE instrument (488 nm). This gave r_{eff} values of between 0.26 and 0.33 μm, with a mean r_{eff} of

0.30 μm. For spheroids and cylinders with an r_{eff} value of 0.29 μm, Liu and Mishchenko (2001) calculate a depolarisation signal of at least 10 %, unless the crystallised particles had a very low degree of asphericity (< 1.1–1.2). A value of 18 % was previously found for crystallisation of oxalic acid aerosols with similar size distributions (Wagner et al., 2010) (Exp. 2 in Fig. 4 therein).

The detection limit for a change in depolarisation at AIDA is about 1 %. No such change in δ was observed during experiments with the aerosols used here or in the previous work with citric acid aerosol (Murray et al., 2010b), strongly suggesting the absence of crystallisation. If we assume that the crystallized particles have the same size and refractive index and a reasonable depolarisation ratio of about 0.2 for these particles then 5 % of the aerosol particles in the chamber would need to crystallise in order to produce a detectable change in depolarisation. A similar fraction of crystallites would also be required for detection with FTIR extinction measurements. One might therefore argue that the heterogeneous ice crystal modes observed in our study were due to nucleation on a small subset of particles which had crystallized instead of forming a glassy solid. However, the following experimental data provides strong evidence that this was not the case.

In order to further test if the solution aerosol were crystallising we performed a dedicated experiment with raffinose aerosol in which raffinose solution was injected at ~ 241 K and the resultant aerosol was cooled to 217.5 K over a period of ~ 6 h before warming the chamber to 229 K, at which point an expansion experiment was performed (Fig. 4a). If raffinose had crystallised during injection of the aerosol or during the subsequent temperature cycling, it would most likely have nucleated ice heterogeneously like other crystalline materials such as ammonium sulphate (Wise et al., 2009; Abbatt et al., 2006) and oxalic acid (Wagner et al., 2010, 2011). During the expansion, no significant heterogeneous ice nucleation was observed, with < 1 cm^{-3} ice particles nucleating prior to a rapid increase in N_{ice} when the chamber RH$_i$ was within 2 % of the predicted homogeneous freezing threshold (based on AIDA freezing data for liquid H$_2$SO$_4$ solution aerosol, Möhler et al., 2003) (Fig. 4b). This offers very strong evidence that the raffinose aerosol did not crystallise at low temperature and that any heterogeneous nucleation observed in other experiments was not due to crystalline raffinose.

Further experimental evidence of the lack of crystallisation of the glassy aerosols used in this study come from our companion paper Wagner et al. (2012). In that study, run 1C (Fig. 5 therein) took place at ~ 232 K using HMMA aerosol that had previously heterogeneously nucleated ice when in the glassy state at a lower temperature (in run 1B). In run 1C, only significant homogeneous ice nucleation was observed. This shows that the glassy aerosol had liquefied on warming. Had the aerosol been crystalline it would still have been expected to nucleate ice heterogeneously. Similarly, our
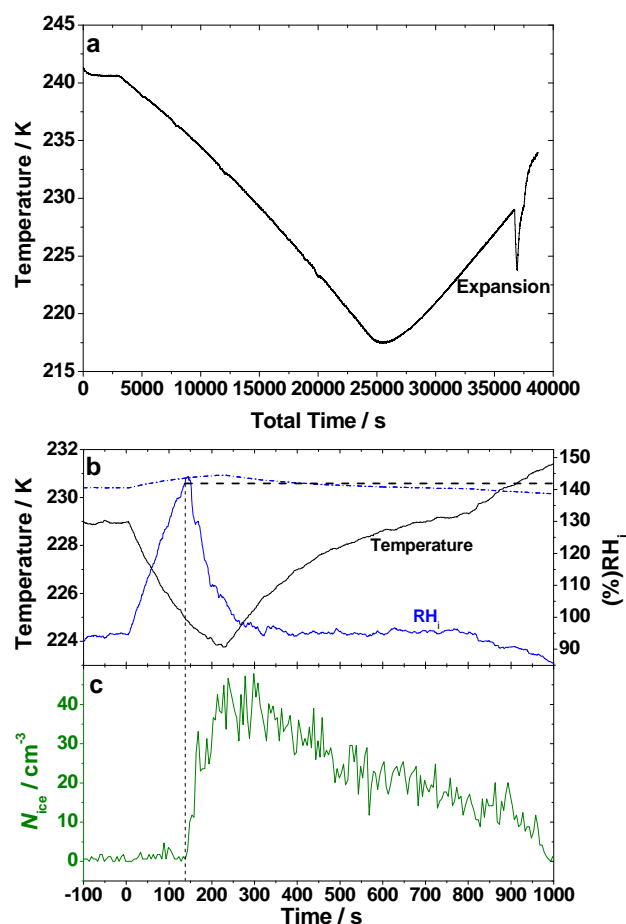

Fig. 4. Panel (**a**) shows the experimental temperature/time series for raffinose aerosol cooled to 217.5 K then warmed up to 229 K at which point an expansion was performed. Panel (**b**) shows the temperature and RH$_i$ (solid black and blue lines respectively) as well as the temperature dependent threshold humidity at which homogeneous ice nucleation is expected to occur, based on AIDA experiments using liquid aqueous H$_2$SO$_4$ aerosol (Möhler et al., 2003) (dot-dash blue line). Panel (**c**) shows the ice particle number concentration, N_{ice}. Homogeneous ice nucleation was observed at the predicted humidity, indicating that the aerosol had liquefied on exposure to increasing humidity, which would not have occurred had it crystallised.

companion paper also shows the results of an expansion performed on raffinose/M5AS aerosol particles at ~ 216 K (run 4A, Fig. 12 therein), that had previously nucleated ice when glassy. Again, after warming into the liquid regime, the only significant ice formation occurred homogeneously. This again strongly indicates that the heterogeneous nucleation at lower temperatures was by glassy particles which were able to liquefy on warming rather than by crystallites. In both cases, to ensure that those particles that nucleated ice in the first run were not lost by sedimentation, ice crystals
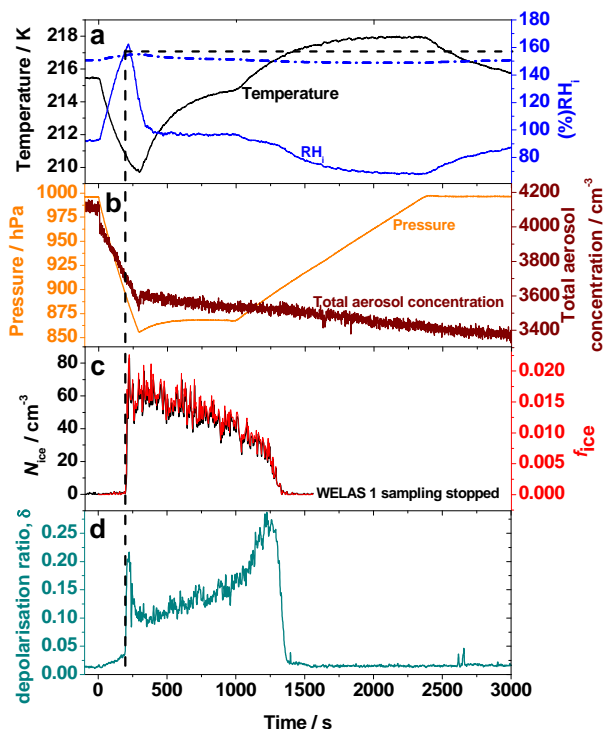
Fig. 5. A typical expansion experiment at the AIDA chamber using liquid aqueous raffinose/M5AS aerosol. Panel **(a)** shows the temperature and RH_i (solid black and blue lines) as well as the expected homogeneous freezing RH_i (dash-dot blue line), based on AIDA homogeneous freezing data from liquid aqueous H_2SO_4 aerosol (Möhler et al., 2003). Panel **(b)** shows the pressure and total aerosol concentration (orange and burgundy lines). The ice particle number concentration from WELAS 1 and the fraction of aerosol that froze are shown in **(c)** (black and red lines). In **(d)**, the onset of ice nucleation is seen as the sharp rise in δ (cyan line). The time/humidity at the onset of freezing is marked with dashed black lines.

were sublimed quickly by refilling the chamber immediately after pumping had stopped.

These experiments and the literature discussed above strongly suggest that solute crystallisation from the aqueous solution aerosols did not occur and instead the aerosols were in either a liquid, semi-solid or glassy state depending on chamber temperature and humidity. Hence, heterogeneous ice nucleation was due to the presence of glassy aerosol particles rather than crystalline particles.

2.2 Materials

The single component aerosols investigated were Raffinose (D-(+)-Raffinose pentahydrate, $\geq 98\%$, 594.52 g mol^{-1}, Sigma-Aldrich), levoglucosan ((−)-1,6-Anhydro-β-D-glucopyranose, $\geq 99\%$, 162.14 g mol^{-1}, Merck Schuchardt) and HMMA (4-Hydroxy-3-methoxy-DL-mandelic acid, 98%, 198.17 g mol^{-1}, Alfa Aesar). The multi component aerosol was a 1 : 1 mixture of raffinose and M5AS – a

mixture of 30.7 wt % malonic acid($\geq 99\%$, 104.06 g mol^{-1}, Merck Schuchardt), 14.7 wt % malic acid (DL-Malic acid, $\geq 99.5\%$, 134.08 g mol^{-1}, Merck), 14.1 wt % maleic acid ($\geq 99\%$, 116.07 g mol^{-1}, Merck Schuchardt), 17.7 wt % glutaric acid ($\geq 99\%$, 132.11 g mol^{-1}, Merck Schuchardt), 7.4 wt % methylsuccinic acid (99%, 132.12 g mol^{-1}, Sigma-Aldrich) and 15.4 wt % ammonium sulphate ($\geq 99.5\%$, 132.14 g mol^{-1}, Merck). All solutions were made using 18.5 MΩ cm water and were passed through a sub-micron (0.45 μm) particulate filter to remove particulates. Raffinose/M5AS, levoglucosan, HMMA and raffinose solution aerosol have T_g' at 209.6 ± 8.1, 211.7 ± 11.1, 236.5 ± 3.5 and 240.6 ± 6.1 K respectively (Zobrist et al., 2008) (see Table 1).

3 Results and discussion

3.1 Expansions with a liquid aerosol

The results of an expansion using raffinose/M5AS solution aerosol are shown in Fig. 5. The aerosol in this experiment was in the liquid state as the chamber gas temperature at the start of the expansion (215.5 K) was well above T_g' (209.6 K). On expansion, the chamber pressure was reduced (orange line, panel b), resulting in initially adiabatic cooling. As the gas temperature dropped, RH_i increased (black and blue lines, Fig. 5a). In order for the water activity of the liquid aerosol particles to remain in equilibrium with the surrounding humidity, they must take up water. In the phase diagram shown in Fig. 3, the arrow from point A to point B is an idealised temperature/water activity trajectory of aerosol during an expansion. Liquid solution aerosol particles become more dilute and freeze when they reach the homogeneous freezing threshold. The onset of freezing was detected first as an increase in the depolarisation ratio, δ (blue line, Fig. 5d). This onset is within ∼5 % of the humidity of homogeneous ice nucleation in sulphuric acid aerosol at the AIDA chamber (Möhler et al., 2003) (dotted blue line, Fig. 5a). Ice particles grew rapidly into the size range detectable by the WELAS 1 instrument (ice particle number concentration, black line, Fig. 5c). The fraction of aerosol that froze (f_{ice}) is similar to f_{ice} found previously for liquid citric acid solution aerosol in an expansion with a similar cooling rate (Murray et al., 2010b). The dilution of liquid aerosol on increasing RH_i followed by homogeneous freezing is the expected behaviour for liquid aerosol particles (Koop et al., 2000; Möhler et al., 2003; Murray et al., 2010b).

After nucleation, the supersaturation in the chamber was rapidly quenched by the growth of ice particles, lowering RH_i to well below the homogeneous ice nucleation threshold preventing any further nucleation. At the end of pumping, heat from the chamber walls (which do not cool significantly during expansions) caused the gas temperature to rise, but the ice cloud persisted. The chamber was returned to its starting pressure by refilling with dry, particulate free

synthetic air. This rapidly reduced RH_i to well below 100 % and completed the sublimation of the ice cloud, returning δ to its starting value.

3.2 Expansions with glassy aerosol

Aerosols in the glassy state showed very different behaviour to that of liquid aerosol. This is illustrated by experiments at different temperatures that used the same HMMA solution aerosol. The aerosol was injected at ∼ 247 K and then subjected to an initial test expansion at a temperature above the homogeneous freezing limit (i.e. no ice was nucleated) and then cooled below T'_g (the experimental temperature profile is shown in Fig. 6a). An expansion was then performed at ∼ 220 K in which depolarisation measurements show that the glassy HMMA aerosol nucleated ice at 120 % RH_i, well below the expected homogeneous limit (Fig. 6b1 and b2). The optical particle counter results show that the fraction of aerosol activated to ice (f_{ice}) increased gradually up to ∼ 0.005, a value similar to that found for heterogeneous ice nucleation by glassy citric acid aerosol (Murray et al., 2010b). This indicates that the glassy HMMA aerosol particles also nucleated ice heterogeneously. The aerosol was then warmed back up to 232 K and underwent another expansion. A concentration of 200 cm^{-3} ice particles nucleated at the homogeneous limit, with only ∼ 1 cm^{-3} nucleating earlier (Fig. 6c1, and c2). There was a corresponding rapid increase in f_{ice}, which reached ∼ 0.05.

These experiments also add further weight to the evidence that the aerosol acted as IN whilst in the glassy state, rather than nucleating ice having crystallised. Had crystallisation occurred in the aerosol population, it would be expected that heterogeneous nucleation would have also been observed in the run at 232 K. The presence of only the homogeneous freezing mode suggests that the glassy aerosol had liquefied before any heterogeneous nucleation could occur (see Sect. 3.3 for more discussion concerning the liquefaction of aerosol during expansions).

3.3 Heterogeneous ice nucleation: a general property of glassy aerosols

Expansion experiments were repeated with aerosol of each of the four chosen compositions at a range of temperatures above and below T'_g (see Table 1 for chemical structures and T'_g). The results of these experiments are summarised in Fig. 7. All aerosol types were found to nucleate ice at humidities below the homogeneous freezing threshold at temperatures well below T'_g, indicating that glassy aerosols of varying chemical composition are capable of heterogeneously nucleating ice.

While nucleation always occurred heterogeneously on glassy aerosol well below T'_g, homogeneous nucleation was observed for raffinose and HMMA aerosols in expansions 11.7 K and 4.3 K below T'_g, respectively. Aerosol particles in
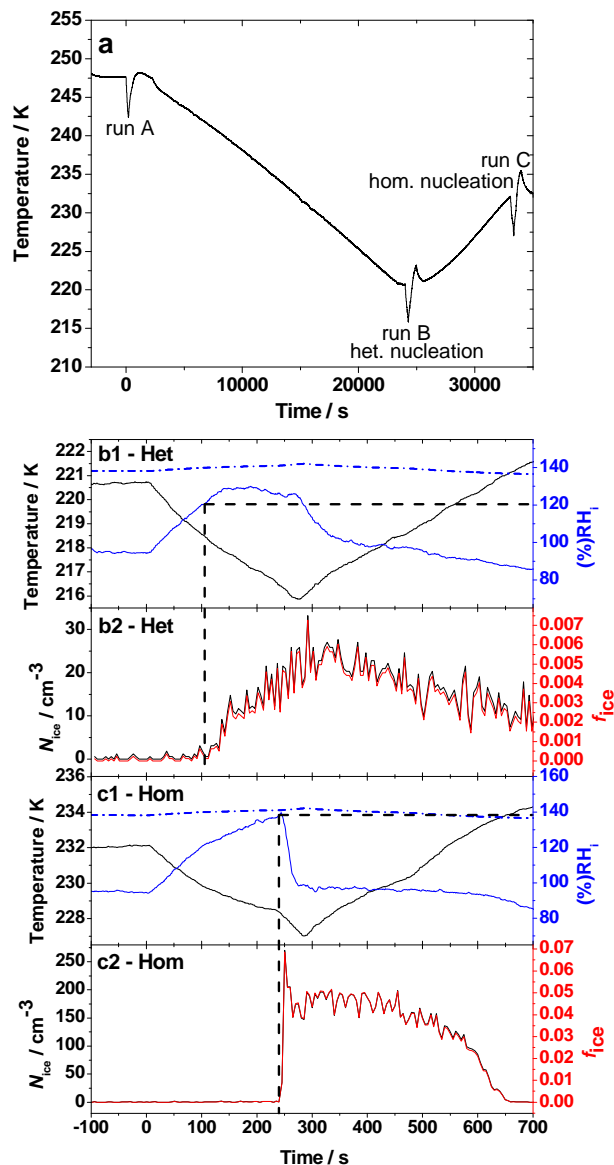

Fig. 6. A comparison of the behaviour of aqueous HMMA solution in expansion runs B and C. Panel **(a)** shows the temperature profile of the experimental series. The bottom panels show experimental data for runs B (started at 220.7 K) and C (started at 232.1 K). Panels **(b1)** and **(c1)** show in each case the experimental temperature and humidity (black and blue solid lines respectively). Panels **(b2)** and **(c2)** show the ice particle number concentration (N_{ice}, black line) and the fraction of the aerosol frozen (f_{ice}, red line). The expected humidity of homogeneous ice nucleation based on liquid sulphuric acid aerosol freezing data (Möhler et al., 2003) is indicated in panels B1 and C1 by dash-dot blue lines. The time/RH_i onsets of ice nucleation are marked with dashed black lines. In each case the onset was observed as an increase of at least 1 % in the backscattering linear depolarisation ratio, which is the most sensitive indicator for the presence of ice particles. This allows the detection of ice particles before they have grown large enough to be counted by the WELAS instruments.
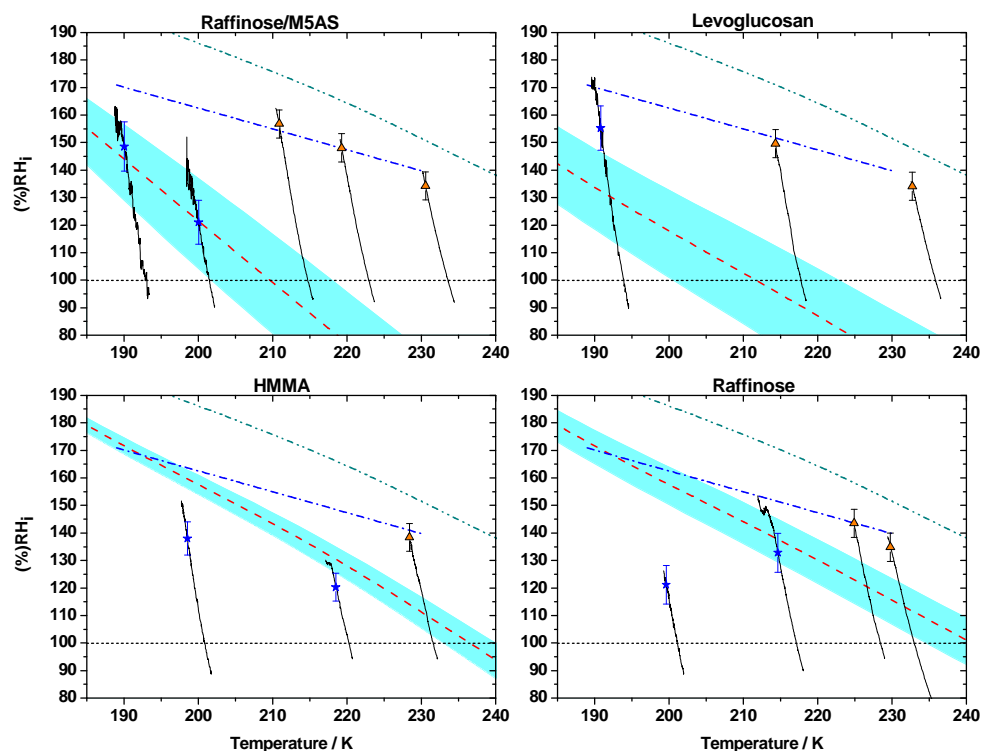
Fig. 7. The experimental temperature – RH_i trajectories for the expansion experiments for each aerosol type (solid black lines). Associated with each trajectory is an ice nucleation onset determined using the depolarisation measurement (defined by a change in the depolarisation ratio of at least 1 % – for example see Fig. 5), with orange triangles representing homogeneous ice nucleation onsets and blue stars representing heterogeneous ice nucleation onsets. The figures also show the aerosol RH_g thresholds (dashed red lines) and their associated uncertainties (shaded blue areas) based on parameterisations from Zobrist et al. (2008). The point at which RH_g crosses the marked 100 % RH_i line (dotted black line) is equal to T'_g for that aerosol type. Also shown is the water saturation line (cyan dot-dot-dash line, shows where RH_{liq} is equal to 100 %) and the expected homogeneous freezing threshold (blue dot-dash line), based on the homogeneous freezing of sulphuric acid solution aerosol in the AIDA chamber (Möhler et al., 2003).

expansions that start close to but still below T'_g may take up water, which serves as a plasticiser, and liquefy on crossing RH_g. This solid-to-liquid transition is also known as amorphous deliquescence (Mikhailov et al., 2009) and may occur before ice can nucleate heterogeneously. Alternatively, the estimates of T'_g could be too high and the aerosol particles may have been liquid to begin with. Given the uncertainty in RH_g it is not possible to categorically rule out either mechanism. However, in the companion paper (Wagner et al., 2012) we show that aerosol particles become pre-activated after the 232 K HMMA and 229–235 K raffinose experiments, which we argue is related to glass formation and suggests that these runs were indeed below T'_g. We suggest that the most likely explanation for homogeneous ice nucleation in the highest temperature HMMA and raffinose runs (despite them starting below RH_g) is that the aerosol particles liquefied before ice was nucleated heterogeneously.

Some differences in the behaviour of aerosols of differing compositions were observed. For example, at ∼ 200 K raffinose/M5AS and raffinose particles both nucleated ice at about 121 % RH_i whereas HMMA aerosol was found to nu-

cleate ice at 137 % RH_i at this temperature. In addition, the two systems with higher T'_g (raffinose and HMMA) nucleated ice at higher temperatures than levoglucosan and the raffinose/M5AS mixture, which have lower T'_g values. For example, at 218.5 K HMMA nucleated ice heterogeneously at 120 % RH_i, whereas levoglucosan and raffinose/M5AS only nucleated ice at the homogeneous limit. The impact of changing the aerosols chemical composition (and consequently T'_g) on the temperature at which the aerosol nucleate ice heterogeneously is further evidence that the ice nucleation observed in this study is governed by the transition of liquid aerosol into glassy solid aerosol. Our findings also show that if atmospheric aerosol were to undergo a glass transition then the temperature and humidity at which the aerosol would nucleate ice would be likely to be dependent upon its chemical composition.

It was, very reasonably, predicted by Zobrist et al. (2008) that glassy aerosols would be unlikely to nucleate ice heterogeneously due to their "smooth convex surface that is disordered on a molecular level". They surmised that such a surface would lack the characteristics of efficient ice nuclei,

such as a crystal lattice match with ice (e.g. silver iodide, Vonnegut, 1947) or surface defects like cracks or pores. This study and the previous study using citric acid aerosol (Murray et al., 2010b) show clearly that a small fraction of glassy aerosol particles of varied compositions are able to act as ice nuclei in the deposition mode. The surfaces of this subset of glassy aerosol may therefore possess some "active sites" that are able to stabilise nascent germs of the ice phase. As suggested by Zobrist et al. (2008), the surface of glassy aerosol particles is less likely to host defects such as cracks or pores that might support a critical germ of ice. However, all the aerosols tested in this study are aqueous solutions of species that have numerous hydrogen bonding sites in the form of OH groups and/or carboxylic acid groups. Both water molecules and the solute species will be present at the surface of the aerosol particles and be available to hydrogen bond to adsorbed water molecules, thus fulfilling the chemical bond requirements of an effective ice nucleus (Pruppacher and Klett, 1997). We propose that ice nucleation by the glassy aerosol in this study is catalysed by water and solute molecules that are arranged in a manner that happens to provide a hydrogen bonding site that matches the crystal lattice of ice. Active sites such as these might occur as in any amorphous material with a degree of short range order (Elliott, 1990) and more ordered regions may serve as a template for ice. Sites capable of nucleating ice may be rare, thus explaining why only small fractions of the glassy aerosols were found to nucleate ice. These active sites may be more or less common in glassy solution aerosol of different chemical composition, which would explain the observed difference in ice nucleation efficiency of the aerosols tested in this study.

All of the aerosols tested in this study have RH_g thresholds that fall entirely or mostly in the predicted RH_g range for SOA (Fig. 1). This implies that the glass forming properties of the solution aerosols used here are comparable to those of atmospheric SOA. There is mounting evidence that SOA generated in chambers and sampled from the atmosphere can nucleate ice in both the deposition and the immersion mode (Knopf et al., 2010; Wang et al., 2012; Möhler et al., 2008). The f_{ice} values for the α-pinene derived SOA particles used by Möhler et al. (2008) are consistent with those observed for citric acid (Murray et al., 2010b) and those for the aerosol investigated in this study (Fig. 8). In their study of amorphous SOA generated by the oxidation of naphthalene by OH radicals and then deposited on a hydrophobic substrate, Wang et al. (2012) observed that the SOA nucleated ice heterogeneously in the deposition mode at temperatures below ~ 230 K. The onset of heterogeneous ice nucleation was observed at between about 135 and 150 % RH_i. Above ~ 230 K, the aerosol particles were observed to take up water on increasing humidity. The change in behaviour of the particles at ~ 230 K was found to be related to the physical state of the aerosol. Deposition nucleation occurred below ~ 230 K
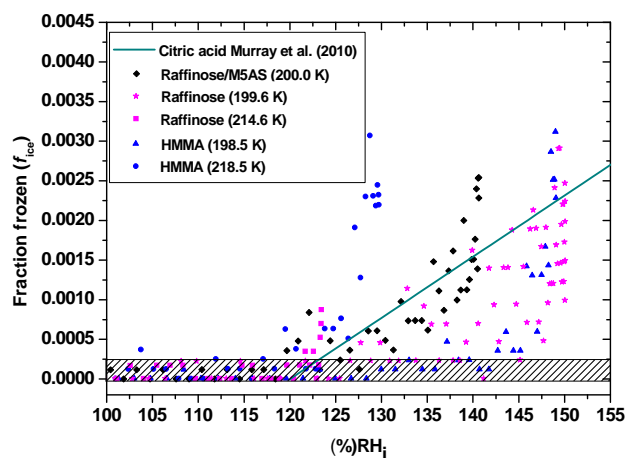

Fig. 8. The fraction of aerosol that froze heterogeneously at temperatures above 198 K during the expansion experiments shown in Fig. 7. At temperatures below 198 K, the ice crystals were too small to allow N_{ice} to be inferred accurately from the WELAS data using a size threshold, preventing the calculation of f_{ice} for those experiments. See figure legend for details. Bracketed numbers in legend indicate the temperature at which the onset of ice nucleation occurred in each case. The solid cyan line is the linear fit ($f_{ice} = 7.7211 \times 10^{-5}$ (% RH_i) $- 9.2688 \times 10^{-3}$ for $RH_i = 121$–170 % and $f_{ice} = 0$ when $RH_i < 121$ %) used in Murray et al. (2010b) to parameterise heterogeneous ice nucleation by glassy citric acid solution aerosol, which was based on experiment 3 from that study, in which the ice onset occurred at 200.5 K. Due to scatter in the ice particle concentration data, a certain amount of noise is present. The shaded region represents a region of uncertainty in which the signal to noise ratio is too low for an accurate estimation of the fraction frozen.

at which temperature the aerosol were thought to be in an amorphous solid state, which is consistent with our findings.

There are also a number of contrasting studies in which no ice nucleation was observed on SOA. Wagner et al. (2007) report no significant heterogeneous ice nucleation by the SOA in their study. Instead, the aerosol were only found to nucleate ice close to water saturation. It was also found that SOA particles generated by the ozonolysis of a variety of alkenes did not nucleate ice heterogeneously in the deposition mode (Prenni et al., 2009). This may simply have been the nature of SOA generated in that experiment or it could be due to the experiments taking place at relatively higher temperatures (243 K), at which the aerosol may have been in a liquid rather than glassy or semi-solid state.

An interesting observation in this study was the apparent continuation of the heterogeneous nucleation of ice particles above the RH_g threshold, i.e. the point at which glassy aerosol could be expected to liquefy. Ice particle production was observed above RH_g for levoglucosan, raffinose/M5AS and raffinose aerosols as well as for citric acid (Murray et al., 2010b). The rate at which glassy aerosol take up water and liquefy is kinetically limited by the diffusion of water from

the surface of the aerosol droplets into the bulk (Zobrist et al., 2011; Koop et al., 2011). Tong et al. (2011) show that this process was delayed by 10–100 s of seconds in supermicron sucrose droplets at room temperature, which might be consistent with our observation of ice particle production above RH_g. It should be noted however, that our experiments used much smaller droplets and took place at much lower temperatures, and therefore deeper into the glassy regime, both of which may well affect any delay in water uptake. In order to explore this, "iso-humid" experiments were performed in which the pumping speed was controlled in order to maintain the chamber humidity at close to constant RH_i (±10 %) above RH_g, but below the homogeneous freezing threshold, for periods on the order of 500 s. In separate expansions using raffinose/M5AS and raffinose particles, starting at 202 K and ∼ 218 K, respectively (Fig. 9), the ice nucleation onsets (vertical dashed black lines) occurred just below or at RH_g (dot-dot-dash red lines) and then ice particle production continued after RH_g was crossed. The ice nucleation onset for the expansion using levoglucosan solution aerosol at ∼ 190 K occurred well above the RH_g threshold (Fig. 7), with ice particle production continuing as pumping went on (not shown).

There are several potential explanations for the nucleation of ice above RH_g but below the homogeneous nucleation threshold. Firstly, at the temperatures at which this behaviour was observed, and also at those found in the upper troposphere, the absolute amount of water vapour for a given relative humidity is much smaller than at room temperature. For this reason, the aerosol may take longer to liquefy than the 10–100 s of seconds found in experiments performed using glassy sucrose droplets at room temperature (Tong et al., 2011). This would also be supported by the observations of Zobrist et al. (2011), who found that sucrose viscosities increased strongly with decreasing temperature. In the presented iso-humid experiments the aerosol could therefore have persisted in the glassy state for the duration of the experiments, allowing them to be available for heterogeneous ice nucleation. To further investigate this possibility, we have estimated the viscosity of the aerosol during the expansion experiments using an approach set out by Murray (2008a, b). The super-Arrhenius dependency of viscosity with temperature (η_T) above the glass transition temperature (T_g) at an RH_i can be approximated by the Williams-Landel-Ferry (WLF) equation:

$$\log \eta_T = \log \eta_{T_g} \left(\frac{17.44 \left[T - T_g \right]}{51.6 + \left[T - T_g \right]} \right) \quad (2)$$

where viscosity is in cP and T is the chamber gas temperature. The numerical values are typical for glass forming systems (Debenedetti, 1996). The molecular diffusion coefficient for the water molecules in the aerosol was then estimated based on the viscosity (converted to Pa s) using the Stokes-Einstein equation:
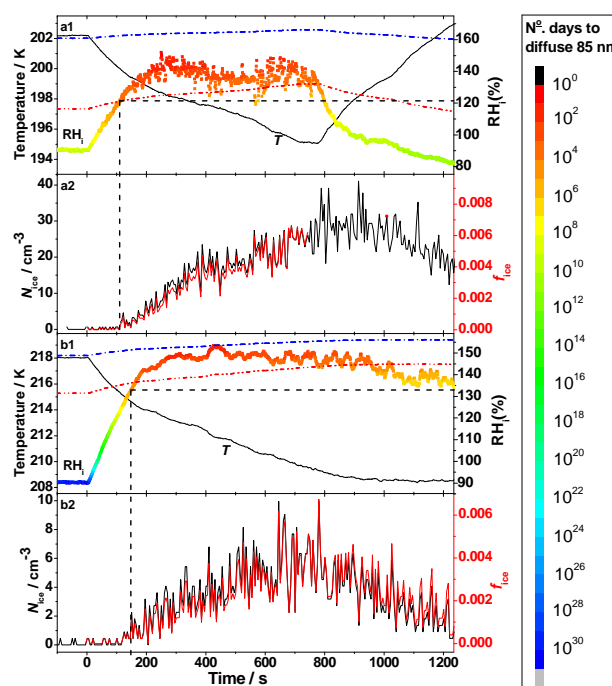

Fig. 9. Time series for ice production runs using raffinose/M5AS solution aerosol **(a1, a2)** and raffinose solution aerosol **(b1, b2)**. The temperature trajectories are shown as solid black lines in panels **(a1)** and **(b1)**. In these panels the RH_i trajectories are displayed as colour mapped time series, the colour maps correspond the estimated time taken for water molecules in the aerosol particles to diffuse 85 nm (the average radius of particles in this study), see Sect. 3.3 for details. The humidity at which homogeneous ice nucleation is expected is shown in both cases as a dash-dot blue line. RH_g is shown as red dot-dot-dash lines. The ice particle number concentration (N_{ice}) and fraction frozen (f_{ice}) are shown as black and red lines respectively. The onset of ice nucleation is represented in each case by black dashed lines.

$$D_{H_2O} = \frac{kT}{6\pi \eta_T r_{H_2O}} \quad (3)$$

where k is the Boltzmann constant and r_{H_2O} is the hydrodynamic radius of water (0.94 Å; Murray, 2008a). Finally, we estimated the time, t, for a water molecule to diffuse a root mean distance (x_i) of 85 nm (the average radius of the aerosols used in this study, see Fig. 2) using the estimated diffusion coefficients:

$$t = \frac{x_i^2}{6 D_{H_2O}} \quad (4)$$

For both the experiments shown in Fig. 9 we have displayed the time to diffuse 85 nm as a colour map overlaid on the RH_i time series in panels a1 and b1. From this it can be seen that even at the highest humidities reached in the two experiments, the time to diffuse 85 nm is estimated at days.

This is much longer than the duration of the experiments, suggesting that the aerosols would not have had time to liquefy.

A second possibility for appearance of ice crystals above RH_g is that all the ice particles nucleated below RH_g but only grew to a sufficiently large size to be counted as an ice particle by the WELAS instruments on a longer time scale. However, growth of ice particles under these conditions is most likely much more rapid than the duration of the iso-humid experiments; Möhler et al. (2006) estimate that the time taken to grow into the size range of the WELAS instruments after nucleation at the homogeneous threshold is 4 s at 223 K, 8 s at 210 K and 50 s at 196 K. Also, the rapid production of ice crystals in the experiments with liquid aerosol indicate that ice growth is unlikely to be a limiting factor. The third possible explanation is that our estimate of the position of the RH_g line is inaccurate and the aerosol remained in a glassy state throughout the experiment. While this possibility is difficult to exclude for the data presented in this paper, experiments with citric acid presented previously (Murray et al., 2010b) show that heterogeneous nucleation continued to a much higher RH_i above the expected RH_g. In the citric acid experiments greater pumping speeds were employed which drove the RH_i to larger values than was possible with the pumping speeds used in this study. Slower pumping speeds were used in the present study to avoid reaching the homogeneous freezing threshold and therefore avoided the risk of pre-activating the aerosol (see companion paper, Wagner et al., 2012). In the citric acid experiments ice particles were produced up to $\sim 40 \% RH_i$ above our best estimate of RH_g which suggests that the uncertainties in the ice nucleation onset humidity which were on the order of 15 % RH_i cannot account for the nucleation of ice above the estimated RH_g line.

Ice production at constant humidity might imply that the time dependence of nucleation on glassy aerosol is significant. Indeed, recent work on ice nucleation in the immersion mode by mineral dusts shows that time dependence may be significant under atmospherically relevant conditions (Murray et al., 2011, 2012b; Broadley et al., 2012). This may be important in the TTL, because under the weakly forced conditions found in this region a parameterisation neglecting time dependence (i.e. a singular parameterisation) may under predict the number of ice nuclei. However, in order to generate iso-humid conditions the temperature was constantly dropping in order to compensate for the loss of water vapour to the growing ice crystals. Hence, it is not possible to separate any time dependence from possible temperature dependence in these experiments, despite the RH_i remaining constant. Further work should be carried out to establish the time dependence of ice nucleation by glassy aerosol and for now we provide a singular description for the parameterisation of ice nucleation by glassy aerosol.

3.4 Parameterising ice nucleation by glassy aerosol

Modelling studies are required to gauge the importance of glassy aerosol in the nucleation of cirrus ice particles. The impact of heterogeneous ice nucleation by glassy aerosol on cirrus cloud properties at TTL temperatures has been modelled previously by Murray et al. (2010b). That study used a one dimensional cloud model and represented glassy aerosol using a parameterisation based on a linear fit to the fraction of glassy citric acid solution aerosol which nucleated ice heterogeneously (f_{ice}) during an expansion experiment at the AIDA chamber at ~ 200 K between 121 and 170 % RH_i. Here we compare f_{ice} for aerosols tested in this study to the citric acid parameterisation. The parameter f_{ice} can only be used accurately if the size distribution in the application is similar to the size distribution of aerosol particles in the experiments. To aid the prediction of the ice nucleation behaviour of aerosols with differing size distributions, we have calculated the ice active surface site density (n_s) (Connolly et al., 2009). This parameter takes into consideration the aerosol surface area and we present humidity and temperature dependent n_s values for each glassy system. We also compare n_s for glassy aerosol particles with other materials for which n_s values are reported in the literature.

3.4.1 Parameterisations based on the fraction activated to ice (f_{ice})

A comparison of f_{ice} for aerosols that nucleated ice heterogeneously at temperatures $\geq \sim 200$ K with the parameterisation for citric acid is shown in Fig. 8. Data are shown up to the point at which the relative humidity reached a maximum. Peak RH_i in an expansion experiment is determined by the pumping speed and the number of ice crystals nucleated as well as the humidity at which they start nucleating. In general, the greater the pumping speed the higher the peak RH_i. As mentioned earlier, the peak RH_i in the published citric acid experiments (Murray et al., 2010b) was larger than that achieved here because the pumping speeds used were greater.

3.4.2 Parameterisations based on the ice active surface site density (n_s)

Nucleation is a stochastic time dependent process (Vonnegut and Baldwin, 1984; Broadley et al., 2012; Murray et al., 2011, 2012b), but it has been suggested that the time dependence of nucleation is of secondary importance when compared to particle heterogeneity (Pruppacher and Klett, 1997; Vali, 2008). The assumption of time independence underpins the singular model and provides a simple way to parameterise ice nucleation data. Connolly et al. (2009) define n_s as $n_s = -\ln(1 - f_{ice})/\sigma$, where σ is the surface area of the aerosol present during an experiment. This is similar to the volume based cumulative nucleus spectrum defined by Vali (1971, 1994). The ice active surface site density has been

applied to a number of other experimental studies of different deposition ice nuclei (Connolly et al., 2009; Saunders et al., 2010; Steinke et al., 2011; Niemand et al., 2012). It is a particularly useful quantity as it provides a surface area independent measurement of a materials ability to nucleate ice. It should be noted that when the singular approximation is applied to conditions of much slower cooling rate than were employed in the experiment upon which the parameterisation was based, the description may lead to an underestimate of the number of ice nuclei (Murray et al., 2011, 2012b; Vonnegut and Baldwin, 1984).

In order to estimate the ice active surface site density for glassy aerosols in our experiments it was assumed that the glassy particles were spherical in shape, and the total surface area of the aerosol was then estimated from size distributions taken prior to the start of expansion (Fig. 2). The loss of aerosol particles during expansion has been accounted for in our calculation by scaling the total surface area with the total aerosol number.

The ice active surface site density for expansion experiments with glassy aerosol, including citric acid (based on the parameterisation of f_{ice} from a previous campaign, (Murray et al., 2010b) (discussed above), are compared in Fig. 10. For the glassy aerosols tested in this study, n_s values at the onset of nucleation were similar ($\sim 6 \times 10^8\,\mathrm{m}^{-2}$). As humidity rose, new ice particles nucleated and there is a corresponding increase in n_s. Peak n_s values varied, but for most glassy aerosols the maximum values were in the region of $\sim 1 \times 10^{10}\,\mathrm{m}^{-2}$. Note that the peak n_s depended on the maximum supersaturation attained in an experiment; for example, in the experiment with glassy raffinose aerosol at 199.6 K (magenta stars), pumping was discontinued earlier and this resulted in smaller maximum n_s values ($\sim 2.5 \times 10^9\,\mathrm{m}^{-2}$). The rate of increase of n_s with RH_i and the humidity at which nucleation was first detected were dependent on composition of the aerosol and also the temperature at which the expansion took place. One notable difference is that the expansions with HMMA aerosol had a more rapid rate of increase of n_s as the humidity increased than was found for the other glassy systems. Fits to all of the calculated n_s values shown in Fig. 10 are given in Table 2.

The range of observed onset humidities makes the parameterisation of glassy aerosol for modelling purposes nontrivial. The atmospheric aerosol particles in a particular location are likely to have a range of compositions and any that are glassy are likely therefore to have a range of ice nucleating abilities. Ice nucleation will be dominated by the ice nuclei in the aerosol that can catalyse ice formation at the lowest humidities. Since citric acid is amongst the materials which nucleate ice at the lowest humidity it seems sensible to use the parameterisation for ice nucleation on aqueous citric acid in cirrus models. In addition, the fit to citric acid is valid over the widest range of RHs which also lends itself to use in models.
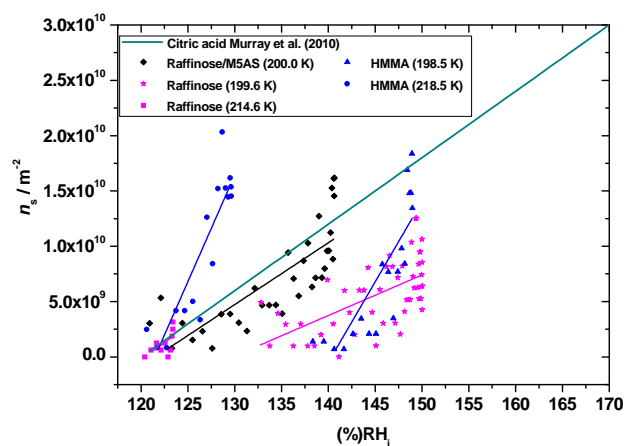

Fig. 10. The ice active surface site densities (n_s) for glassy aerosols which nucleated ice heterogeneously (see Fig. 7). Linear fits to each dataset are shown in the corresponding colour. The solid cyan line is n_s for glassy citric acid aerosol calculated using the fraction frozen parameterisation from Murray et al. (2010b) (shown in Fig. 8) and the size distribution for the aerosol used in the experiment upon which the parameterisation is based. Table 2 contains equations for linear fits to n_s for aerosols from this study and glassy citric acid aerosol.

For comparison, n_s data for other atmospherically relevant ice nuclei is shown together with n_s data for glassy aerosol in Fig. 11. Arizona Test Dust (ATD, grey triangles) (Connolly et al., 2009), volcanic ash from the Eyjafjallajökull eruption (grey circles) (Steinke et al., 2011) and iron oxide nanoparticles (dashed grey line) (Saunders et al., 2010) have higher n_s values and are therefore more efficient ice nuclei than glassy aerosol per unit of surface area. While mineral dust is clearly a more effective ice nucleus, the number density (and therefore surface area) of aerosol particles which are potentially glassy far exceeds that of mineral dust in the upper troposphere (Froyd et al., 2010).

3.5 The impact of glassy aerosol on cirrus formation outside the TTL

The results presented here show that glassy aerosol can nucleate ice under conditions relevant for ice cloud formation in parts of the atmosphere which are warmer than the very cold TTL. In the following lines we explore the possibility that ice nucleation on glassy aerosol might compete with ice nucleation on mineral dusts at warmer cirrus temperatures. Starting with a total of $300\,\mathrm{cm}^{-3}$ aerosol particles and, based on the measurements of DeMott et al. (2003) that 1% of these were mineral dust particles and 86% were organic sulphate particles. We assume that mineral dust particles have a diameter of 500 nm and the organic-sulphate particles have a diameter of 150 nm. We also assume that only 50% of the organic-sulphate aerosol particles are glassy and that 50% of the mineral dust particles have been deactivated by coatings.

Table 2. Parameters for the linear fits to n_s shown in Fig. 10 and Fig. 11 as a function of RH_i. Also included is n_s for glassy citric acid aerosol, calculated based on a parameterisation of f_{ice} vs. RH_i (Murray et al., 2010). Note that each fit is only valid for the range of RH_i shown in the rightmost column of the table.

| Aerosol	Temperature of ice nucleation onset/K	Linear fit ($n_s = m \cdot RH_i + c$)		Valid RH_i range for fit
		m	c	
Raffinose/M5AS	200.0	5.5815×10^8	-6.7861×10^{10}	$120.9 \leq RH_i \leq 140.6$
Raffinose	199.6	6.15127×10^8	-7.4095×10^{10}	$120.4 \leq RH_i \leq 123.4$
Raffinose	214.6	3.65814×10^8	-4.74938×10^{10}	$132.8 \leq RH_i \leq 150.0$
HMMA	198.5	1.45114×10^9	-2.03713×10^{11}	$138.3 \leq RH_i \leq 149.0$
HMMA	218.5	1.92381×10^9	-2.33764×10^{11}	$120.6 \leq RH_i \leq 129.6$
Citric acid	200.5	6.00235×10^8	-7.20796×10^{10}	$121.0 \leq RH_i \leq 170.0$
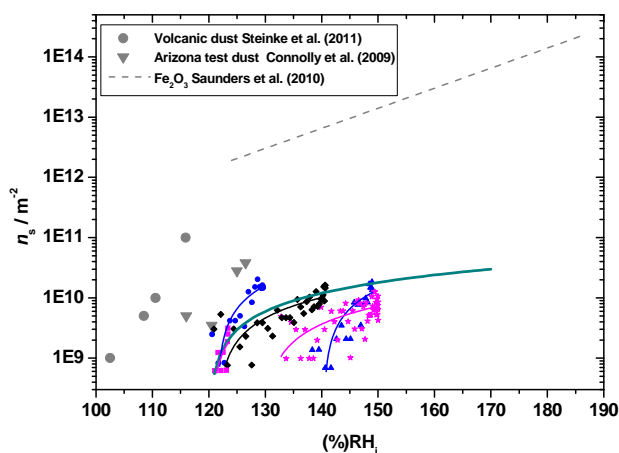
Fig. 11. A comparison of n_s for glassy aerosols from this study and other IN species (see Fig. 8 legend for symbol details). Glassy citric acid aerosol n_s is also shown (Murray et al., 2010a) (solid cyan line, see Fig. 10 caption for details). Linear fits to the data from this study are shown in the corresponding colour. Volcanic dust at ~ 225 K, (grey circles) (Steinke et al., 2011), Arizona test dust (ATD) at 238–248 K (grey downwards pointing triangles) (Connolly et al., 2009) (note that these are revised figures for ATD, based on a re-analysis by Niemand et al., 2012) and a parameterisation of n_s for iron oxide nanoparticles at 190 K (grey dashed line) (Saunders et al., 2010) are shown. The parameters to the fits to n_s vs. RH_i for all of the glassy aerosols shown in this figure (solid lines) are included in Table 2.

Using an n_s value for mineral dust of 3×10^{10} m^{-2} and a value of 3×10^9 m^{-2} for sulphate-organic aerosol at 125 % RH_i (see Fig. 11), we estimate that mineral dust and organic-sulphate particles would nucleate comparable numbers of ice particles (0.033 vs. 0.027 cm^{-3}). The total number of ice particles nucleated would be ~ 0.060 cm^{-3}, which is consistent with the observed mean ice particle number density in mid-latitude cirrus (Krämer et al., 2009). This estimation suggests amorphous solid organic aerosol could play a role in mid-latitude cirrus formation.

4 Conclusions

The main aim of this study was to compare the ice nucleating properties of a range of atmospherically relevant glass forming compounds under conditions relevant for cirrus cloud formation. In a previous study (Murray et al., 2010b) glassy citric acid solution aerosol particles were found to nucleate ice heterogeneously at temperatures below T_g' (the glass transition temperature at ice saturation, 100 % RH_i). In this study we tested the ice nucleation efficiency of atmospherically relevant aerosol species with T_g' close to that of citric acid (raffinose/M5AS and levoglucosan solution aerosols) and species with much higher T_g' (raffinose and HMMA solution aerosols). At temperatures ≤ 200 K all the aerosol types acted as heterogeneous ice nuclei, catalysing ice production below the homogeneous freezing threshold (Fig. 7). Raffinose and HMMA aerosol, which form glasses at temperature above 200 K were also found to nucleate ice heterogeneously at higher temperatures (214.6 K and 218.5 K respectively). These results suggest that heterogeneous ice nucleation is a general property of glassy aerosols and that the temperature at which they are able to nucleate ice is strongly related to their glass transition temperature.

In a very recent study Baustian et al. (2011) used Raman microscopy in conjunction with a humidity controlled cold stage to investigate the ice nucleation properties of aqueous super-micron sized glassy particles. It was found that glassy sucrose, dextrose and citric acid solution particles nucleate ice heterogeneously in the deposition mode. In addition, Wang et al. (2012) have also shown that SOA particles generated by the oxidation of naphthalene by OH radicals heterogeneously nucleate ice in the deposition mode when in an amorphous solid state. These results support our conclusion that heterogeneous ice nucleation is a general property of aqueous glassy aerosol particles.

The onset humidity of heterogeneous ice formation was found to be dependent on both the temperature and the chemical composition of the aerosol used. With the exception of raffinose aerosol, the heterogeneous ice nucleation onsets increased at lower temperatures. A wide range of onset

humidities were observed; for instance glassy levoglucosan aerosol nucleated ice at 155 % RH_i at 190.8 K whereas glassy HMMA aerosol nucleated ice heterogeneously at 120 % RH_i at 218.5 K.

This study shows that irrespective of their composition, aerosols in the glassy state are very likely to nucleate ice heterogeneously at temperatures relevant to the TTL (≤ 200 K). In-situ analysis of the residue from sub-visible cirrus ice particles from the TTL found the vast majority of residues were indistinguishable from the mixed sulphate-organic aerosol that makes up the bulk of the sampled unfrozen aerosol (Froyd et al., 2009b, 2010). This was in contrast to cirrus formed from anvil cloud outflows, in which a high proportion of ice particles residues contained mineral dust particles. A number of studies (e.g. Virtanen et al., 2010) show that atmospheric SOA and other aerosol containing organic material exists in an amorphous solid or semisolid state. The glassy aerosols that were observed to nucleate ice in this study all have humidity dependent glass transition thresholds (RH_g) that sit within the range predicted for SOA by Koop et al. (2011) (Fig. 1). It is hence likely that a fraction of the observed TTL mixed sulphate-organic aerosol is present in the glassy state and is able therefore to nucleate ice heterogeneously in the same manner as the aerosols tested in this study. This would be consistent with the findings of Froyd et al. (2010) since heterogeneous ice nucleation by glassy aerosol would give ice particle residues that are indistinguishable from the unfrozen interstitial aerosol of the TTL. It would also be consistent with studies which show that the low ice particle concentrations found in TTL cirrus are the result of the clouds forming via heterogeneous rather than homogeneous ice nucleation (Krämer et al., 2009; Gensch et al., 2008; Khvorostyanov et al., 2006; Spichtinger and Gierens, 2009; Spichtinger and Cziczo, 2010; Jensen et al., 2010; Murray et al., 2010b; Ren and Mackenzie, 2005).

The range of observed onset humidities makes the parameterisation of glassy aerosol for modelling purposes non-trivial. Aerosol particles that nucleate ice at lower humidities are likely to be the dominant source of ice particles in a cloud, as early nucleation is likely to prevent the humidity rising significantly. The lowest humidity onsets for ice nucleation were found for Raffinose, HMMA and the raffinose/M5AS aerosol which were all found to nucleate ice at humidities as low as ~ 120 % RH_i, which is consistent with the onsets found for glassy citric acid aerosol (Murray et al., 2010b). For modelling ice nucleation by glassy aerosol we recommend using the parameterisation of the ice active surface site density, n_s, of glassy citric acid aerosol as a function of RH_i (Table 2), which is based on data from Murray et al. (2010b). It is a representation of the properties found in this study and we suggest its use as a basis for ice nucleation by the most active glassy aerosol particles which play an important role in ice formation in cirrus clouds.

References

Abbatt, J. P. D., Benz, S., Cziczo, D. J., Kanji, Z., Lohmann, U., and Mohler, O.: Solid ammonium sulfate aerosols as ice nuclei: A pathway for cirrus cloud formation, Science, 313, 1770–1773, doi:10.1126/science.1129726, 2006.

Adachi, K. and Buseck, P. R.: Atmospheric tar balls from biomass burning in mexico, J. Geophys. Res.-Atmos., 116, D05204, doi:10.1029/2010jd015102, 2011.

Alexander, D. T. L., Crozier, P. A., and Anderson, J. R.: Brown carbon spheres in east asian outflow and their optical properties, Science, 321, 833–836, doi:10.1126/science.1155296, 2008.

Angell, C. A.: Formation of glasses from liquids and biopolymers, Science, 267, 1924–1935, doi:.1126/science.267.5206.1924, 1995.

Angell, C. A.: Liquid fragility and the glass transition in water and aqueous solutions, Chem. Rev., 102, 2627–2649, doi:10.1021/cr000689q, 2002.

Baker, M. B.: Cloud microphysics and climate, Science, 276, 1072–1078, doi:10.1126/science.276.5315.1072, 1997.

Barahona, D. and Nenes, A.: Dynamical states of low temperature cirrus, Atmos. Chem. Phys., 11, 3757–3771, doi:10.5194/acp-11-3757-2011, 2011

Baustian, K. J., Wise, M. E., and Tolbert, M. A.: Depositional ice nucleation on solid ammonium sulfate and glutaric acid particles, Atmos. Chem. Phys., 10, 2307–2317, doi:10.5194/acp-10-2307-2010, 2010.

Baustian, K. J., Wise, M. E., and Tolbert, M. A.: Influence of glassy organic species on ice nucleation and water uptake of single micron-sized aerosol particles, American Geophysical Union Fall Meeting, 2011.

Benz, S., Megahed, K., Möhler, O., Saathoff, H., Wagner, R., and Schurath, U.: T-dependent rate measurements of homogeneous ice nucleation in cloud droplets using a large atmospheric simulation chamber, Journal of Photochemistry and Photobiology a-Chemistry, 176, 208–217, doi:10.1016/j.jphotochem.2005.08.026, 2005.

Bodsworth, A., Zobrist, B., and Bertram, A. K.: Inhibition of efflorescence in mixed organic-inorganic particles at temperatures less than 250 k, Phys. Chem. Chem. Phys., 12, 12259–12266, 2010.

Bogdan, A. and Molina, M. J.: Why does large relative humidity with respect to ice persist in cirrus ice clouds?, J. Phys. Chem. A, 113, 14123–14130, doi:10.1021/jp9063609, 2009.

Bogdan, A. and Molina, M. J.: Aqueous aerosol may build up an elevated upper tropospheric ice supersaturation and form mixed-phase particles after freezing, J. Phys. Chem. A, 114, 2821–2829, doi:10.1021/jp9086656, 2010.

Broadley, S. L., Murray, B. J., Herbert, R. J., Atkinson, J. D., Dobbie, S., Malkin, T. L., Condliffe, E., and Neve, L.: Immersion mode heterogeneous ice nucleation by an illite rich powder representative of atmospheric mineral dust, Atmos. Chem. Phys., 12, 287–307, doi:10.5194/acp-12-287-2012, 2012.

Cappa, C. D. and Wilson, K. R.: Evolution of organic aerosol mass spectra upon heating: implications for OA phase and partitioning behavior, Atmos. Chem. Phys., 11, 1895–1911, doi:10.5194/acp-11-1895-2011, 2011.

Chan, M. N., Choi, M. Y., Ng, N. L., and Chan, C. K.: Hygroscopicity of water-soluble organic compounds in atmospheric aerosols: Amino acids and biomass burning derived organic species, Environ. Sci. Technol., 39, 1555–1562, doi:10.1021/es049584l, 2005.

Chatterjee, K., Shalaev, E. Y., and Suryanarayanan, R.: Raffinose crystallization during freeze-drying and its impact on recovery of protein activity, Pharmaceut. Res., 22, 303–309, doi:10.1007/s11095-004-1198-y, 2005.

Connolly, P. J., Möhler, O., Field, P. R., Saathoff, H., Burgess, R., Choularton, T., and Gallagher, M.: Studies of heterogeneous freezing by three different desert dust samples, Atmos. Chem. Phys., 9, 2805–2824, doi:10.5194/acp-9-2805-2009, 2009.

Debenedetti, P. G.: Metastable liquids : Concepts and principles, Princeton University Press, Princeton, NJ, xiv, 411 pp., 1996.

Debenedetti, P. G. and Stillinger, F. H.: Supercooled liquids and the glass transition, Nature, 410, 259–267, 2001.

Decesari, S., Fuzzi, S., Facchini, M. C., Mircea, M., Emblico, L., Cavalli, F., Maenhaut, W., Chi, X., Schkolnik, G., Falkovich, A., Rudich, Y., Claeys, M., Pashynska, V., Vas, G., Kourtchev, I., Vermeylen, R., Hoffer, A., Andreae, M. O., Tagliavini, E., Moretti, F., and Artaxo, P.: Characterization of the organic composition of aerosols from Rondônia, Brazil, during the LBA-SMOCC 2002 experiment and its representation through model compounds, Atmos. Chem. Phys., 6, 375–402, doi:10.5194/acp-6-375-2006, 2006.

DeMott, P. J., Cziczo, D. J., Prenni, A. J., Murphy, D. M., Kreidenweis, S. M., Thomson, D. S., Borys, R., and Rogers, D. C.: Measurements of the concentration and composition of nuclei for cirrus formation, P. Natl. Acad. Sci. USA, 100, 14655–14660, doi:10.1073/pnas.2532677100, 2003.

Eastwood, M. L., Cremel, S., Wheeler, M., Murray, B. J., Girard, E., and Bertram, A. K.: Effects of sulfuric acid and ammonium sulfate coatings on the ice nucleation properties of kaolinite particles, Geophys. Res. Lett., 36, L02811, doi:10.1029/2008gl035997, 2009.

Elliott, S. R.: Physics of amorphous materials, Longman Scientific & Technical, 1990.

Fahey, D. W., Gao, R. S., and Möhler, O.: Summary of the aquavit water vapor intercomparison: Static experiments, available online at: https://aquavit.icg.kfa-juelich.de/AquaVit/, 2009.

Froyd, K. D., Murphy, D. M., Jensen, E. J., Murray, B. J., and Möhler, O.: Ice nucleation at the tropical tropopause: Insights from *in situ* measurements, simulations and laboratory studies, ICNAA, Prague, Czech Republic, 2009a.

Froyd, K. D., Murphy, D. M., Sanford, T. J., Thomson, D. S., Wilson, J. C., Pfister, L., and Lait, L.: Aerosol composition of the tropical upper troposphere, Atmos. Chem. Phys., 9, 4363–4385, doi:10.5194/acp-9-4363-2009, 2009b.

Froyd, K. D., Murphy, D. M., Lawson, P., Baumgardner, D., and Herman, R. L.: Aerosols that form subvisible cirrus at the tropical tropopause, Atmos. Chem. Phys., 10, 209–218, doi:10.5194/acp-10-209-2010, 2010.

Fueglistaler, S., Dessler, A. E., Dunkerton, T. J., Folkins, I., Fu, Q., and Mote, P. W.: Tropical tropopause layer, Rev. Geophys., 47, RG1004, doi:10.1029/2008rg000267, 2009.

Gao, R. S., Popp, P. J., Fahey, D. W., Marcy, T. P., Herman, R. L., Weinstock, E. M., Baumgardner, D. G., Garrett, T. J., Rosenlof, K. H., Thompson, T. L., Bui, P. T., Ridley, B. A., Wofsy, S. C., Toon, O. B., Tolbert, M. A., Karcher, B., Peter, T., Hudson, P. K., Weinheimer, A. J., and Heymsfield, A. J.: Evidence that nitric acid increases relative humidity in low-temperature cirrus clouds, Science, 303, 516–520, doi:10.1126/science.1091255, 2004.

Gensch, I. V., Bunz, H., Baumgardner, D. G., Christensen, L. E., Fahey, D. W., Herman, R. L., Popp, P. J., Smith, J. B., Troy, R. F., Webster, C. R., Weinstock, E. M., Wilson, J. C., Peter, T., and Kramer, M.: Supersaturations, microphysics and nitric acid partitioning in a cold cirrus cloud observed during cr-ave 2006: An observation-modelling intercomparison study, Environ. Res. Lett., 3, 9, 035003, doi:10.1088/1748-9326/3/3/035003, 2008.

Gordon, M. and Taylor, J. S.: Ideal copolymers and the 2nd-order transitions of synthetic rubbers 1. Non-crystalline copolymers, J. Appl. Chem., 2, 493–500, 1952.

Gunthe, S. S., King, S. M., Rose, D., Chen, Q., Roldin, P., Farmer, D. K., Jimenez, J. L., Artaxo, P., Andreae, M. O., Martin, S. T., and Pöschl, U.: Cloud condensation nuclei in pristine tropical rainforest air of Amazonia: size-resolved measurements and modeling of atmospheric aerosol composition and CCN activity, Atmos. Chem. Phys., 9, 7551–7575, doi:10.5194/acp-9-7551-2009, 2009.

Hansen, J. E. and Travis, L. D.: Light-scattering in planetary atmospheres, Space Sci. Rev., 16, 527–610, doi:10.1007/bf00168069, 1974.

Hinds, W. C.: Aerosol technology: Properties, behavior, and measurement of airborne particles, Wiley, 1999.

Holton, J. R. and Gettelman, A.: Horizontal transport and the dehydration of the stratosphere, Geophys. Res. Lett., 28, 2799–2802, 2001.

Hungerford, E. H. and Nees, A. R.: Raffinose – preparation and properties, Industrial and Engineering Chemistry, 26, 462–464, 1934.

Iinuma, Y., Brueggemann, E., Gnauk, T., Mueller, K., Andreae, M. O., Helas, G., Parmar, R., and Herrmann, H.: Source characterization of biomass burning particles: The combustion of selected european conifers, african hardwood, savanna grass, and german and indonesian peat, J. Geophys. Res.-Atmos., 112, D08209, doi:10.1029/2006jd007120, 2007.

Jensen, E. J., Toon, O. B., Pfister, L., and Selkirk, H. B.: Dehydration of the upper troposphere and lower stratosphere by subvisible cirrus clouds near the tropical tropopause, Geophys. Res. Lett., 23, 825–828, 1996.

Jensen, E. J., Pfister, L., Bui, T.-P., Lawson, P., and Baumgardner, D.: Ice nucleation and cloud microphysical properties in tropical tropopause layer cirrus, Atmos. Chem. Phys., 10, 1369–1384, doi:10.5194/acp-10-1369-2010, 2010.

Johari, G. P., Hallbrucker, A., and Mayer, E.: The glass liquid transition of hyperquenched water, Nature, 330, 552–553, doi:10.1038/330552a0, 1987.

Katkov, II and Levine, F.: Prediction of the glass transition temperature of water solutions: Comparison of different models, Cryobi-

ology, 49, 62–82, doi:10.1016/j.cryobiol.2004.05.004, 2004.

Khvorostyanov, V. I., Morrison, H., Curry, J. A., Baumgardner, D., and Lawson, P.: High supersaturation and modes of ice nucleation in thin tropopause cirrus: Simulation of the 13 july 2002 cirrus regional study of tropical anvils and cirrus layers case, J. Geophys. Res.-Atmos., 111, D02201, doi:10.1029/2004jd005235, 2006.

Knopf, D. A. and Rigg, Y. J.: Homogeneous ice nucleation from aqueous inorganic/organic particles representative of biomass burning: Water activity, freezing temperatures, nucleation rates, J. Phys. Chem. A, 115, 762–773, doi:10.1021/jp109171g, 2011.

Knopf, D. A., Wang, B., Laskin, A., Moffet, R. C., and Gilles, M. K.: Heterogeneous nucleation of ice on anthropogenic organic particles collected in mexico city, Geophys. Res. Lett., 37, L11803, doi:10.1029/2010gl043362, 2010.

Kohl, I., Bachmann, L., Hallbrucker, A., Mayer, E., and Loerting, T.: Liquid-like relaxation in hyperquenched water at $<= 140$ k, Phys. Chem. Chem. Phys., 7, 3210–3220, doi:10.1039/b507651j, 2005.

Koop, T., Luo, B. P., Tsias, A., and Peter, T.: Water activity as the determinant for homogeneous ice nucleation in aqueous solutions, Nature, 406, 611–614, 2000.

Koop, T., Bookhold, J., Shiraiwa, M., and Pöschl, U.: Glass transition and phase state of organic compounds: Dependency on molecular properties and implications for secondary organic aerosols in the atmosphere, Phys. Chem. Chem. Phys., 13, 19238–19255, doi:10.1039/c1cp22617g, 2011.

Krämer, M., Schiller, C., Afchine, A., Bauer, R., Gensch, I., Mangold, A., Schlicht, S., Spelten, N., Sitnikov, N., Borrmann, S., de Reus, M., and Spichtinger, P.: Ice supersaturations and cirrus cloud crystal numbers, Atmos. Chem. Phys., 9, 3505–3522, doi:10.5194/acp-9-3505-2009, 2009.

Liou, K. N.: Influence of cirrus clouds on weather and climate processes – a global perspective, Mon. Weather Rev., 114, 1167–1199, doi:10.1175/1520-0493(1986)114¡1167:ioccow¿2.0.co;2, 1986.

Liu, L. and Mishchenko, M. I.: Constraints on psc particle microphysics derived from lidar observations, J. Quant. Spectrosc. Ra., 70, 817–831, doi:10.1016/s0022-4073(01)00048-6, 2001.

Lynch, D. K., Sassen, K., Starr, D. O. C., and Stephens, G.: Cirrus, Oxford University Press, Cambridge, New York, xvii, 480 pp., 2002.

Magee, N., Moyle, A. M., and Lamb, D.: Experimental determination of the deposition coefficient of small cirrus-like ice crystals near-50 degrees C, Geophys. Res. Lett., 33, L17813, doi:10.1029/2006gl026665, 2006.

Malkin, T. L., Murray, B. J., Brukhno, A. V., Anwar, J., and Salzmann, C. G.: Structure of ice crystallized from supercooled water, P. Natl. Acad. Sci. USA, 109, 1041–1045, doi:10.1073/pnas.1113059109, 2012.

McFarquhar, G. M., Heymsfield, A. J., Spinhirne, J., and Hart, B.: Thin and subvisual tropopause tropical cirrus: Observations and radiative impacts, J. Atmos. Sci., 57, 1841–1853, doi:10.1175/1520-0469(2000)057<1841:TASTTC>2.0.CO;2, 2000.

Mikhailov, E., Vlasenko, S., Martin, S. T., Koop, T., and Pöschl, U.: Amorphous and crystalline aerosol particles interacting with water vapor: conceptual framework and experimental evidence for restructuring, phase transitions and kinetic limitations, At-

mos. Chem. Phys., 9, 9491–9522, doi:10.5194/acp-9-9491-2009, 2009.

Möhler, O., Stetzer, O., Schaefers, S., Linke, C., Schnaiter, M., Tiede, R., Saathoff, H., Krämer, M., Mangold, A., Budz, P., Zink, P., Schreiner, J., Mauersberger, K., Haag, W., Kärcher, B., and Schurath, U.: Experimental investigation of homogeneous freezing of sulphuric acid particles in the aerosol chamber AIDA, Atmos. Chem. Phys., 3, 211–223, doi:10.5194/acp-3-211-2003, 2003.

Möhler, O., Field, P. R., Connolly, P., Benz, S., Saathoff, H., Schnaiter, M., Wagner, R., Cotton, R., Krämer, M., Mangold, A., and Heymsfield, A. J.: Efficiency of the deposition mode ice nucleation on mineral dust particles, Atmos. Chem. Phys., 6, 3007–3021, doi:10.5194/acp-6-3007-2006, 2006.

Möhler, O., Benz, S., Saathoff, H., Schnaiter, M., Wagner, R., Schneider, J., Walter, S., Ebert, V., and Wagner, S.: The effect of organic coating on the heterogeneous ice nucleation efficiency of mineral dust aerosols, Environ. Res. Lett., 3, 025007, doi:10.1088/1748-9326/3/2/025007, 2008.

Murphy, D. M. and Koop, T.: Review of the vapour pressures of ice and supercooled water for atmospheric applications, Q. J. Roy. Meteor. Soc., 131, 1539–1565, doi:10.1256/qj.04.94, 2005.

Murray, B. J.: Enhanced formation of cubic ice in aqueous organic acid droplets, Environ. Res. Lett., 3, 025008, doi:10.1088/1748-9326/3/2/025008, 2008a.

Murray, B. J.: Inhibition of ice crystallisation in highly viscous aqueous organic acid droplets, Atmos. Chem. Phys., 8, 5423–5433, doi:10.5194/acp-8-5423-2008, 2008b.

Murray, B. J. and Bertram, A. K.: Strong dependence of cubic ice formation on droplet ammonium to sulfate ratio, Geophys. Res. Lett., 34, L16810, doi:10.1029/2007gl030471, 2007.

Murray, B. J. and Bertram, A. K.: Inhibition of solute crystallisation in aqueous H^+-NH_4^+-SO_4^{2-}-H_2O droplets, Phys. Chem. Chem. Phys., 10, 3287–3301, doi:10.1039/b802216j, 2008.

Murray, B. J. and Jensen, E. J.: Homogeneous nucleation of amorphous solid water particles in the upper mesosphere, J. Atm. Sol.-Terr. Phys., 72, 51–61, 2010.

Murray, B. J., Knopf, D. A., and Bertram, A. K.: The formation of cubic ice under conditions relevant to earth's atmosphere, Nature, 434, 202–205, doi:10.1038/nature03403, 2005.

Murray, B. J., Broadley, S. L., Wilson, T. W., Bull, S. J., Wills, R. H., Christenson, H. K., and Murray, E. J.: Kinetics of the homogeneous freezing of water, Phys. Chem. Chem. Phys., 12, 10380–10387, 2010a.

Murray, B. J., Wilson, T. W., Dobbie, S., Cui, Z. Q., Al-Jumur, S., Möhler, O., Schnaiter, M., Wagner, R., Benz, S., Niemand, M., Saathoff, H., Ebert, V., Wagner, S., and Karcher, B.: Heterogeneous nucleation of ice particles on glassy aerosols under cirrus conditions, Nature Geosci., 3, 233–237, doi:10.1038/ngeo817, 2010b.

Murray, B. J., Broadley, S. L., Wilson, T. W., Atkinson, J. D., and Wills, R. H.: Heterogeneous freezing of water droplets containing kaolinite particles, Atmos. Chem. Phys., 11, 4191–4207, doi:10.5194/acp-11-4191-2011, 2011.

Murray, B. J., Haddrell, A. E., Peppe, S., Davies, J. F., Reid, J. P., O'Sullivan, D., Price, H. C., Kumar, R., Saunders, R. W., Plane, J. M. C., Umo, N. S., and Wilson, T. W.: Glass formation and unusual hygroscopic growth of iodic acid solution droplets with relevance for iodine mediated particle formation in

the marine boundary layer, Atmos. Chem. Phys., 12, 8575–8587, doi:10.5194/acp-12-8575-2012, 2012a.

Murray, B. J., O'Sullivan, D., Atkinson, J. D., and Webb, M. E.: Ice nucleation by particles immersed in supercooled cloud droplets, Chem. Soc. Rev., 41, 6519–6554, doi:10.1039/C2CS35200A, 2012b.

Niemand, M., Möhler, M., Vogel, B., Vogel, H., Hoose, C., Connolly, P., Klein, H., Bingemer, H., DeMott, P., Skrotzki, J., and Leisner, T.: A particle-surface-area-based parameterization of immersion freezing on mineral dust particles, J. Atmos. Sci., doi:10.1175/JAS-D-11-0249.1, 2012.

Peter, T., Marcolli, C., Spichtinger, P., Corti, T., Baker, M. B., and Koop, T.: When dry air is too humid, Science, 314, 1399–1402, doi:10.1126/science.1135199, 2006.

Posfai, M., Gelencser, A., Simonics, R., Arato, K., Li, J., Hobbs, P. V., and Buseck, P. R.: Atmospheric tar balls: Particles from biomass and biofuel burning, J. Geophys. Res.-Atmos., 109, D06213, doi:10.1029/2003jd004169, 2004.

Prenni, A. J., Petters, M. D., Faulhaber, A., Carrico, C. M., Ziemann, P. J., Kreidenweis, S. M., and DeMott, P. J.: Heterogeneous ice nucleation measurements of secondary organic aerosol generated from ozonolysis of alkenes, Geophys. Res. Lett., 36, L06808, doi:10.1029/2008gl036957, 2009.

Pruppacher, H. R. and Klett, J. D.: Microphysics of clouds and precipitation, 2nd rev. and enl. ed., Atmospheric and oceanographic sciences library, v. 18, Kluwer Academic Publishers, Dordrecht; Boston, 954 pp., 1997.

Ren, C. and Mackenzie, A. R.: Cirrus parametrization and the role of ice nuclei, Q. J. Roy. Meteor. Soc., 131, 1585–1605, doi:10.1256/qj.04.126, 2005.

Roth, C. M., Goss, K. U., and Schwarzenbach, R. P.: Sorption of a diverse set of organic vapors to urban aerosols, Environ. Sci. Technol., 39, 6638–6643, doi:10.1021/es0503837, 2005.

Saukko, E., Lambe, A. T., Massoli, P., Koop, T., Wright, J. P., Croasdale, D. R., Pedernera, D. A., Onasch, T. B., Laaksonen, A., Davidovits, P., Worsnop, D. R., and Virtanen, A.: Humidity-dependent phase state of SOA particles from biogenic and anthropogenic precursors, Atmos. Chem. Phys., 12, 7517–7529, doi:10.5194/acp-12-7517-2012, 2012.

Saunders, R. W., Möhler, O., Schnaiter, M., Benz, S., Wagner, R., Saathoff, H., Connolly, P. J., Burgess, R., Murray, B. J., Gallagher, M., Wills, R., and Plane, J. M. C.: An aerosol chamber investigation of the heterogeneous ice nucleating potential of refractory nanoparticles, Atmos. Chem. Phys., 10, 1227–1247, doi:10.5194/acp-10-1227-2010, 2010.

Schnaiter, M., Büttner, S., Möhler, O., Skrotzki, J., Vragel, M., and Wagner, R.: Influence of particle size and shape on the backscattering linear depolarisation ratio of small ice crystals – cloud chamber measurements in the context of contrail and cirrus microphysics, Atmos. Chem. Phys. Discuss., 12, 15453–15502, doi:10.5194/acpd-12-15453-2012, 2012.

Shilling, J. E., Tolbert, M. A., Toon, O. B., Jensen, E. J., Murray, B. J., and Bertram, A. K.: Measurements of the vapor pressure of cubic ice and their implications for atmospheric ice clouds, Geophys. Res. Lett., 33, L17801, doi:10.1029/2006gl026671, 2006a.

Shilling, J. E., Fortin, T. J., and Tolbert, M. A.: Depositional ice nucleation on crystalline organic and inorganic solids, J. Geophys. Res.-Atmos., 111, D12204, doi:10.1029/2005jd006664, 2006b.

Shiraiwa, M., Ammann, M., Koop, T., and Pöschl, U.: Gas uptake and chemical aging of semisolid organic aerosol particles, P. Natl. Acad. Sci. USA, 108, 11003–11008, doi:10.1073/pnas.1103045108, 2011.

Skrotzki, J.: High-accuracy multiphase humidity measurements using tdlas: Application to the investigation of ice growth in simulated cirrus clouds, Doctor of Natural Sciences, Combined Faculties for the Natural Sciences and for Mathematics, Ruperto-Carola University of Heidelberg, Heidelberg, 140 pp., 2012.

Spichtinger, P. and Cziczo, D. J.: Impact of heterogeneous ice nuclei on homogeneous freezing events in cirrus clouds, J. Geophys. Res.-Atmos., 115, D14208, doi:10.1029/2009jd012168, 2010.

Spichtinger, P. and Gierens, K. M.: Modelling of cirrus clouds – Part 2: Competition of different nucleation mechanisms, Atmos. Chem. Phys., 9, 2319–2334, doi:10.5194/acp-9-2319-2009, 2009.

Steinke, I., Möhler, O., Kiselev, A., Niemand, M., Saathoff, H., Schnaiter, M., Skrotzki, J., Hoose, C., and Leisner, T.: Ice nucleation properties of fine ash particles from the Eyjafjallajökull eruption in April 2010, Atmos. Chem. Phys., 11, 12945–12958, doi:10.5194/acp-11-12945-2011, 2011.

Tivanski, A. V., Hopkins, R. J., Tyliszczak, T., and Gilles, M. K.: Oxygenated interface on biomass burn tar balls determined by single particle scanning transmission x-ray microscopy, J. Phys. Chem. A, 111, 5448–5458, doi:10.1021/jp070155u, 2007.

Tong, H.-J., Reid, J. P., Bones, D. L., Luo, B. P., and Krieger, U. K.: Measurements of the timescales for the mass transfer of water in glassy aerosol at low relative humidity and ambient temperature, Atmos. Chem. Phys., 11, 4739–4754, doi:10.5194/acp-11-4739-2011, 2011.

Vaden, T. D., Imre, D., Beranek, J., Shrivastava, M., and Zelenyuk, A.: Evaporation kinetics and phase of laboratory and ambient secondary organic aerosol, P. Natl. Acad. Sci. USA, 108, 2190–2195, doi:10.1073/pnas.1013391108, 2011.

Vali, G.: Supercooling of water and nucleation of ice (drop freezer), Am. J. Phys., 39, 1125, doi:10.1119/1.1976585, 1971.

Vali, G.: Freezing rate due to heterogeneous nucleation, J. Atmos. Sci., 51, 2683–2683, 1994.

Vali, G.: Repeatability and randomness in heterogeneous freezing nucleation, Atmos. Chem. Phys., 8, 5017–5031, doi:10.5194/acp-8-5017-2008, 2008.

Vargaftik, N. B., Volkov, B. N., and Voljak, L. D.: International tables of the surface-tension of water, J. Phys. Chem. Ref. Data, 12, 817–820, 1983.

Virtanen, A., Joutsensaari, J., Koop, T., Kannosto, J., Yli-Pirila, P., Leskinen, J., Makela, J. M., Holopainen, J. K., Pöschl, U., Kulmala, M., Worsnop, D. R., and Laaksonen, A.: An amorphous solid state of biogenic secondary organic aerosol particles, Nature, 467, 824–827, doi:10.1038/nature09455, 2010.

Vonnegut, B.: The nucleation of ice formation by silver iodide, J. Appl. Phys., 18, 593–595, doi:10.1063/1.1697813, 1947.

Vonnegut, B. and Baldwin, M.: Repeated nucleation of a supercooled water sample that contains silver iodide particles, J. Clim. Appl. Meteorol., 23, 486–490, doi:10.1175/1520-0450(1984)023¡0486:rnoasw¿2.0.co;2, 1984.

Wagner, R., Benz, S., Möhler, O., Saathoff, H., and Schurath, U.: Probing ice clouds by broadband mid-infrared extinction spectroscopy: case studies from ice nucleation experiments in the AIDA aerosol and cloud chamber, Atmos. Chem. Phys., 6, 4775–

4800, doi:10.5194/acp-6-4775-2006, 2006.

Wagner, R., Benz, S., Möhler, O., Saathoff, H., Schnaiter, M., and Leisner, T.: Influence of particle aspect ratio on the midinfrared extinction spectra of wavelength-sized ice crystals, J. Phys. Chem. A, 111, 13003–13022, doi:10.1021/jp0741713, 2007

Wagner, R., Linke, C., Naumann, K. H., Schnaiter, M., Vragel, M., Gangl, M., and Horvath, H.: A review of optical measurements at the aerosol and cloud chamber aida, J. Quant. Spectrosc. Ra., 110, 930–949, doi:10.1016/j.jqsrt.2009.01.026, 2009.

Wagner, R., Möhler, O., Saathoff, H., Schnaiter, M., and Leisner, T.: High variability of the heterogeneous ice nucleation potential of oxalic acid dihydrate and sodium oxalate, Atmos. Chem. Phys., 10, 7617–7641, doi:10.5194/acp-10-7617-2010, 2010.

Wagner, R., Möhler, O., Saathoff, H., Schnaiter, M., and Leisner, T.: New cloud chamber experiments on the heterogeneous ice nucleation ability of oxalic acid in the immersion mode, Atmos. Chem. Phys., 11, 2083–2110, doi:10.5194/acp-11-2083-2011, 2011.

Wagner, R., Möhler, O., Saathoff, H., Schnaiter, M., Skrotzki, J., Leisner, T., Wilson, T. W., and Murray, B. J.: Ice cloud processing of ultra-viscous/glassy aerosol particles leads to enhanced ice nucleation ability, Atmos. Chem. Phys., 12, 8589–8610, doi:10.5194/acp-12-8589-2012, 2012.

Wagner, W. and Pruss, A.: The iapws formulation 1995 for the thermodynamic properties of ordinary water substance for general and scientific use, J. Phys. Chem. Ref. Data, 31, 387–535, 2002.

Wan, E. C. H. and Yu, J. Z.: Analysis of sugars and sugar polyols in atmospheric aerosols by chloride attachment in liquid chromatography/negative ion electrospray mass spectrometry, Environ. Sci. Technol., 41, 2459–2466, doi:10.1021/es062390g, 2007.

Wang, B., Lambe, A. T., Massoli, P., Onasch, T. B., Davidovits, P., Worsnop, D. R., and Knopf, D. A.: The deposition ice nucleation and immersion freezing potential of amorphous secondary organic aerosol: Pathways for ice and mixed phase cloud formation, J. Geophys. Res., 117, D16209, doi:10.1029/2012JD018063, 2012.

Wise, M. E., Baustian, K. J., and Tolbert, M. A.: Laboratory studies of ice formation pathways from ammonium sulfate particles, Atmos. Chem. Phys., 9, 1639–1646, doi:10.5194/acp-9-1639-2009, 2009.

Wise, M. E., Baustian, K. J., and Tolbert, M. A.: Internally mixed sulfate and organic particles as potential ice nuclei in the tropical tropopause region, P. Natl. Acad. Sci. USA, 107, 6693–6698, doi:10.1073/pnas.0913018107, 2010.

Wise, M. E., Baustian, K. J., Koop, T., Freedman, M. A., Jensen, E. J., and Tolbert, M. A.: Depositional ice nucleation onto crystalline hydrated NaCl particles: a new mechanism for ice formation in the troposphere, Atmos. Chem. Phys., 12, 1121–1134, doi:10.5194/acp-12-1121-2012, 2012.

Young, K. D. and Leboeuf, E. J.: Glass transition behavior in a peat humic acid and an aquatic fulvic acid, Environ. Sci. Technol., 34, 4549–4553, doi:10.1021/es000889j, 2000.

Zobrist, B., Marcolli, C., Pedernera, D. A., and Koop, T.: Do atmospheric aerosols form glasses?, Atmos. Chem. Phys., 8, 5221–5244, doi:10.5194/acp-8-5221-2008, 2008.

Zobrist, B., Soonsin, V., Luo, B. P., Krieger, U. K., Marcolli, C., Peter, T., and Koop, T.: Ultra-slow water diffusion in aqueous sucrose glasses, Phys. Chem. Chem. Phys., 13, 3514–3526, doi:10.1039/c0cp01273d, 2011.